Chapter 18

Mechanism of Onset of Liquefaction

The Badshahi Masjid in Lahore of Pakistan, which was constructed by Shah Jahan, the fifth Mughal Emperor.

18.1 Mechanism of Liquefaction

Studies on causative mechanisms of liquefaction were initiated by shaking water-saturated model ground (Maslov, 1957; Florin and Ivanov, 1961; Yoshimi 1967). Although much was found by them, more quantitative study became possible after introducing laboratory shear tests.

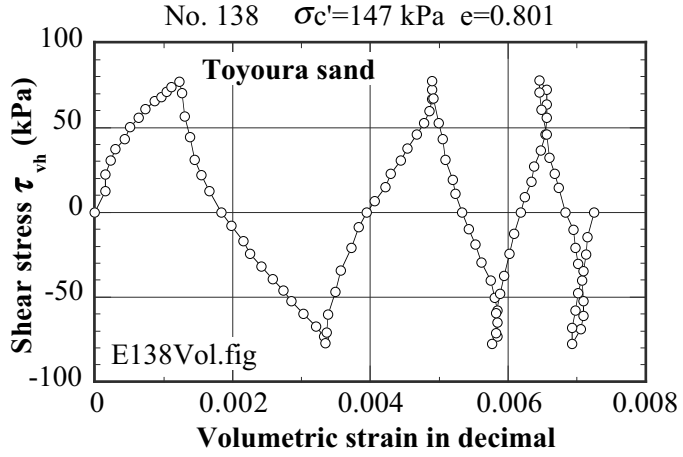

Fig. 18.1 Volume decrease of loose sand during cyclic drained shear

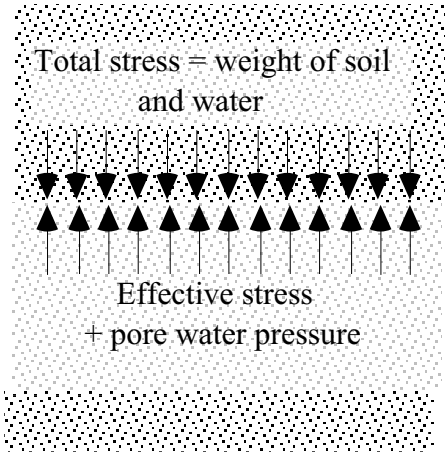

Fig. 18.2 Calculation of effective stress

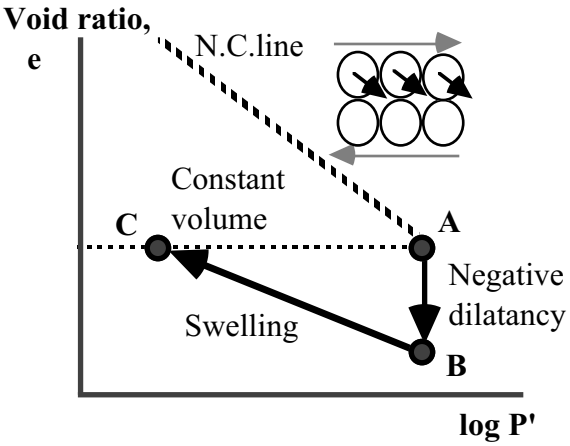

Fig. 18.3 Negative dilatancy

Figure 18.1 indicates the volume contraction 体積収縮 of loose Toyoura sand undergoing cyclic drained shear. This volume change induced by shear is called negative dilatancy (Sect. 1.6). If sand is saturated, pore water is drained out of sand upon this cyclic volume contraction.

In real earthquake loading, drained cyclic shear and immediate volume contraction are unlikely. When a sand deposit is of several meters in thickness, the time required for drainage is 10–30 min (see Sect. 17.3), which is much longer than the duration time of earthquake loading (10–20 s, approximately). It is thus reasonable to consider real sandy ground to be undrained during earthquake shaking. When there is a thin clayey impervious layer, furthermore, it prevents seepage and drainage from underlying deposits toward the surface.

When shear occurs under undrained conditions, pore water cannot be drained out, and develops pressure. This pressure is called the excess pore water pressure 過剰間隙水圧 and is defined as the pore water pressure minus the hydrostatic pressure that existed before earthquake;

$$\text{Excess pore water pressure} = \text{Pore water pressure} - \text{Hydrostatic pressure}, \tag{18.1}$$

which is identical with (1.4). The contact force between sand grains is called the effective stress and controls the rigidity and shear strength of soil (Sects. 1.3 and 1.5). The effective stress is calculated by

$$\text{Effective stress} = \text{Total stress} - \text{Pore water pressre} \tag{18.2}$$

Since the total stress is equal to the weight of soil above the concerned elevation, it does not change with time (Fig. 18.2). Accordingly, the effective stress decreases when pore water pressure increases.

Consequently, sand becomes softer. When the effective stress reaches zero, there is no more shear strength in sand (Coulomb´s failure criterion, 1.14), sand behaves similar to liquid, and large ground deformation occurs. The high excess pore water pressure is dissipated after tens of minutes. This consolidation procedure results in subsidence of ground (settlement 圧密沈下).

Figure 18.3 illustrates an "*e vs. logP′* " diagram, as originally drawn by Seed (1979), that demonstrates the mechanism of pore pressure rise. Initially, the state of *water-saturated sand* 飽和砂 is at A upon a normal-consolidation line. When sheared, sand tries to contract its volume toward **B**. Since no drainage is allowed, however, the volume and void ratio have to be held constant. Thus, unloading of effective stress is needed to cancel the volume contraction (**AB**) by swelling (**BC**). In reality, the volume contraction (**AB**) and swelling (**BC**) are superimposed, and the state of soil moves directly from **A** to **C**. The volume contraction of **AB** becomes reality after dissipation of developed excess pore water pressure (consolidation settlement; Sects. 17.8 and 18.3).

When the extent of negative dilatancy is more significant, the point B is located further below, and the effective stress at C becomes very small. This is called liquefaction. This occurs when sand is very loose or when the magnitude of cyclic shear is substantial.

When sand is not saturated with water 不飽和砂, pore air is compressed or solves into water. Hence, volume can contract and swelling is not required very much. Hence, effective stress does not decrease very much.

The discussion above suggests not only the mechanism of liquefaction but also the following principles of mitigative measures against liquefaction:

– Densification or compaction of sand in order to reduce negative dilatancy (**AB**)
– Installation of gravel drains to accelerate the rate of drainage
– Grouting to bond grains to each other and prevent particle movement as well as negative dilatancy (Fig. 18.2)
– Preventing large shear strain that leads to high excess pore water pressure
– Lowering of ground water to introduce air into pore space (volume change is allowed)

18.2 Sand Boiling

When the vertical effective stress is zero, the excess pore water pressure at depth z is $(\gamma - \gamma_w)z$. The hydraulic gradient, 動水勾配, is $i = (\gamma/\gamma_w) - 1 = i_{cr}$, which is known as the critical gradient. Consequently, a mixture of sand grain and water is ejected out of ground. In Fig. 18.4, the sand boiling reached the height of 2 m above the surface and the ejected sand is seen on the wall. In the Shinano River, Niigata, and the small inlet in the Lingayen Bay area, the Philippines, many water boilings were observed out of river/sea water (Wakamatsu, 1993). It seems that the energy of ejected water in river/sea beds is stronger than those onshore.

Fig. 18.4 Ejected sand on wall (Dagupan, 1990)

Fig. 18.5 Sand crater after Liquefaction (1994 Hokkaido Nansei-oki earthquake, Hakodate Harbor)

Boiling of water and sand leaves a crater on the ground surface (Fig. 18.5). The ejected sand deposits around the hole of ejection, while water flows away, transporting fine particles together. Coarse grains cannot be transported to the ground surface (Stokes law). Therefore, the grain size in the crater is uniform and fine (100–300 μm), although there are some exceptions. This observation led to an idea in early days that fine uniform sand is most likely to liquefy. In recent years, however, liquefaction of gravelly soils (Sect. 20.2) as well as fine cohesionless soils (Sect. 20.5) attracts concern.

The color of ejected sand is blue to gray, because the sand has been submerged in water until liquefaction, and is not oxidized.

Sangawa (1992) excavated an archaeological site of liquefaction and showed that coarse material was not transported to the ground surface (Fig. 18.6).

Boiling is possible to occur in submarine ground if sand is loose. After the May 25 Noto Peninsula

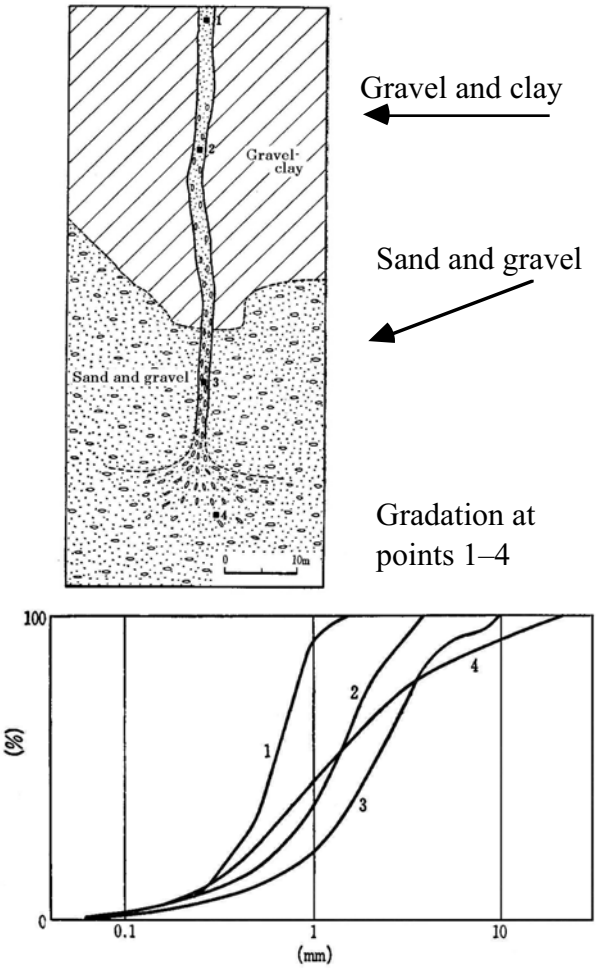

Fig. 18.6 Excavated boiling channel(Sangawa, 1992)

earthquake in Japan (magnitude = 6.9), the Japan Coast Guard conducted detailed surveys on the seabed topography along the submarine seismic fault and detected more than ten topographies that appeared similar to boiling of sand.

18.3 Dissipation of Excess Pore Water Pressure

Figure 18.7 reveals the distribution of excess pore water pressure (not including hydrostatic pressure) observed in a shaking table test. When dissipation is going on, the pressure distribution is bilinear, conformed of $\gamma' \times depth$ in the upper portion, and the constant pressure in the lower part (Fig. 18.8). This point is different from what Terzaghi consolidation theory demonstrated for clay. Dissipation started at the bottom and the range of constant pressure expanded upward with time. It is important that the hydraulic gradient at the surface is equal to the critical gradient i_{cr} (Sect. 1.12) until 28 s (Fig. 18.8) which is most part of the period of dissipation. The duration time of dissipation can be calculated by Darcy´s law (Sect. 1.12);

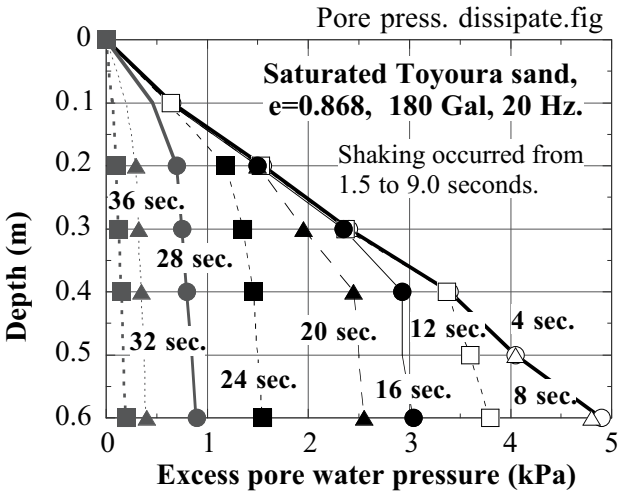

Fig. 18.7 Distribution of pore pressure in 1-G model test (Sundarraj,1996).

Time = (Volume of drained water)/(Rate of water flow)

$$= \left(\varepsilon_v H\right) \Big/ \left(k i_{cr}\right) \qquad (18.3)$$

where ε_v is the volumetric strain after liquefaction (e.g., 0.05 or 5% for loose sand), H the thickness of liquefied sand (60 cm here), k the permeability (0.1 cm/s here), and $i_{cr} = 0.8$ in this text; for definition of i_{cr}, see (1.26). Consequently, the calculated duration time is 37.5 s, which is in good agreement with the observation of around 40 s. Upon Niigata earthquake, sand boiling started at a few minutes after shaking and continued for roughly 20 min (Fig. 18.9 by Mr. Yutaka Takeuchi). The duration time is proportional to H, in contrast to H^2 proportionality in Terzaghi theory. Consequently, the insitu duration time can be as long as 1 h.

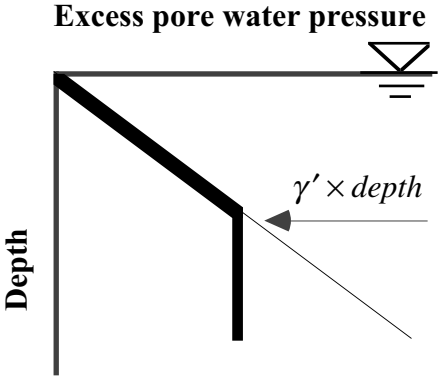

Fig. 18.8 Bilinear idealization of excess pore water variation in vertical direction

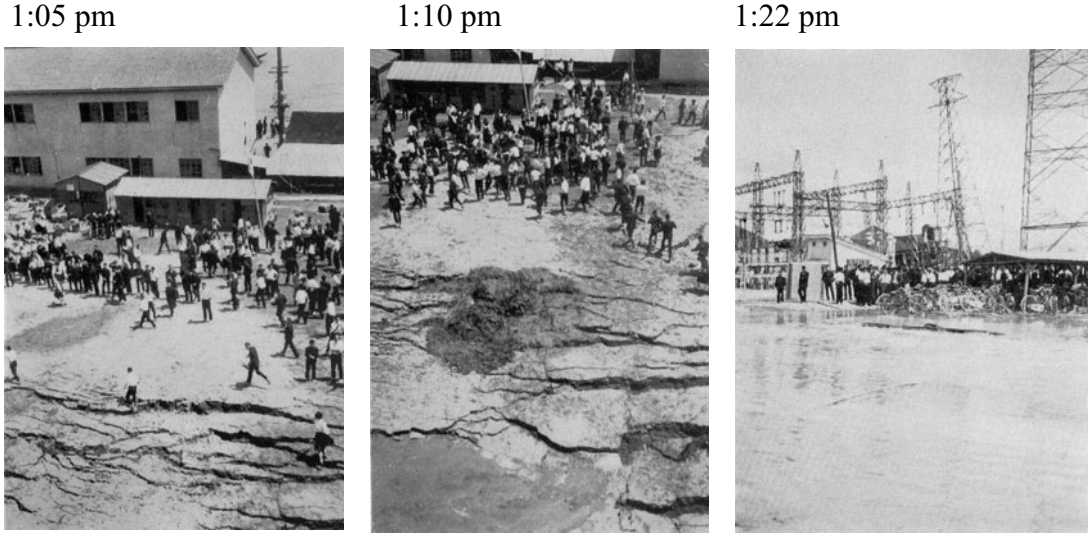

Fig. 18.9 Pictures taken during the 1964 Niigata earthquake (1:02 pm) (Photographs taken by Mr. Yutaka Takeuchi; JSSMFE, 1966)

Sand has a large volume contraction when the effective stress increases slightly from the state of complete liquefaction (Sect. 19.10). This is the reason for the difference from the Terzaghi´s theory (1.12).

18.4 Paleoliquefaction

Liquefaction is an evidence that an earthquake of substantial intensity occurred. A detected sand boil (Sect. 18.2) indicates that a strong earthquake occurred in the particular region at a certain time. Liquefaction is thus a reliable evidence to find ancient earthquakes that are missing in written history or that occurred in prehistoric times (See also Sect. 18.5).

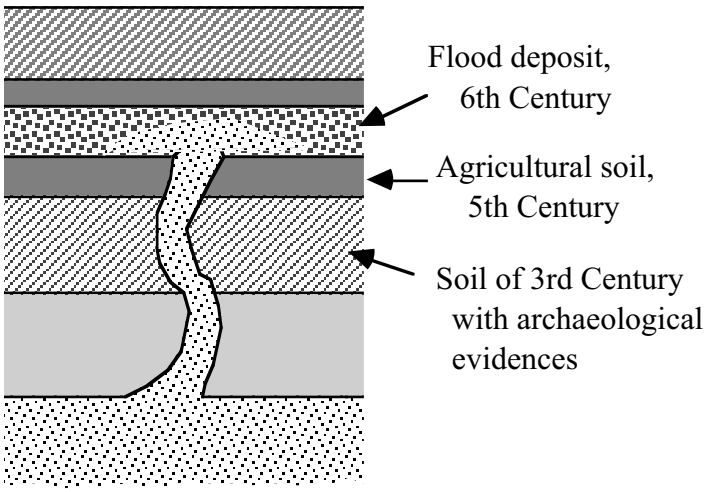

Fig. 18.10 Identification of age of ancient liquefaction

Figure 18.10 illustrates the idea. The excavated sand boil penetrates through soils of third and fifth centuries. Therefore, this liquefaction and the causative earthquake occurred in or after the 5th century. On the other hand, the sand boil is covered by a flood deposit of sixth century. Hence, the earthquake occurred before this flooding. Consequently, it is concluded that a big earthquake took place in fifth or sixth century. The age of soil is identified by using archaeological objects (考古学資料), carbon isotope (C_{14}), tefra chronology (volcanic ash), and others.

By performing this kind of study nationwide, Sangawa (1997) detected many gigantic earthquakes, which had been missing in history. Figure 18.11 summarizes the history of big earthquakes that rocked the western part of Japan in the past more than 1,300 years. Those earthquakes with ● were identified by excavated sand boils and are consistent with known ones in written history. In contrast, those earthquakes with ○ were newly discovered by liquefaction studies. It is important that the newly detected earthquakes such as those in the B zone in 1498 fill the blank of earthquake histories between 1361 and 1605 and indicates more clearly the regular return period of gigantic earthquakes in the subduction zone. Accordingly, it is somehow possible to imagine the time of the next catastrophic earthquake.

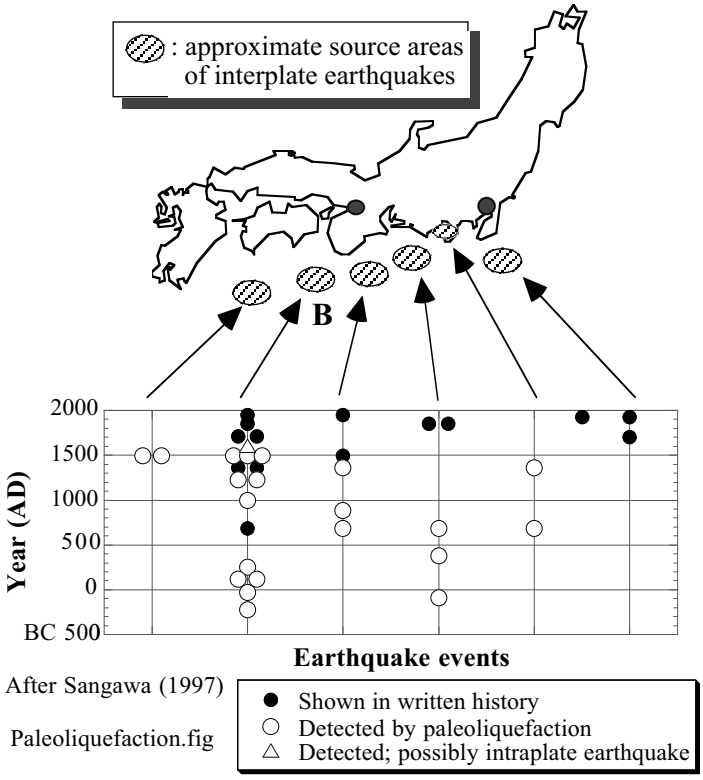

Fig. 18.11 History of gigantic earthquakes in subduction zone of Philippine Sea plate (drawn after Sangawa, 1997)

Paleoliquefaction study is a useful tool to investigate the local seismic activity when no written historical document is available (Elton and Hamou, 1990; Obermeier et al., 1985; Talwani and Cox, 1985; Talwani and Schaeffer, 2001). The paleoliquefaction approach to detect gigantic earthquake has been taken as well in the coastal area of, for example, Washington state of USA (Atwater, 1992).

18.5 Excavation of Buried Sand Boil

Embedded sand boiling is excavated at many places in the recent times. The aim of the excavation is to investigate the history of unrecorded strong earthquakes in the past, to understand the relationship between particle sizes of ejected sand at the surface and those in the original sand layer, and to observe the geometry of sand boiling.

Figure 18.12 is the view of excavation in a river bed in Sekiyado Town of Saitama, Japan, which was carried out by Tobishima Corporation. Figure 18.13 shows the cross section of the excavated ground in which sand boil was detected. The channel of boiled sand is not straight. Tuttle et al. (1990) found an extremely complicated shape of a boiling channel in their excavation study.

Fig. 18.12 Overall view of excavation at liquefaction site in Sekiyado

Fig. 18.13 Channel of boiled sand (Sekiyado)

18.6 Hot Liquefaction; True or Not True

Several past earthquakes were associated with something hot. For example, when Eginitis (1895) reported a big earthquake of 1894 in the Marmara Sea area of Turkey, he quoted eyewitness reports on warm sea water in St. Stephanos, warm well water in Makrikeuy, and rising of ground temperature at Galata. When the same area was hit by the 1999 Kocaeli earthquake, Mr. Beytullah Emen of Degirmendere City had his back injured by something hot when he fell down into the sea upon tsunami attack (Towhata et al. 2001). Tsukuda (1995) cited an eyewitness report that boiling water from liquefaction (Sect. 18.2) was as warm as 50 °C during the 1990 Manjil earthquake, Iran. Wakamatsu (1993) reported that boiled sand and water were warm in Agoo area of the Philippines after the Luzon earthquake in 1990 (Set. 18.14). As for the same earthquake, Hamada et al. (1995) and Tsukuda (1995) mentioned that fish was boiled in a pond when the bottom soil liquefied in the Narbakan area. The author heard about hot liquefaction after the Qayen-Birjand earthquake of Iran in 1997. Finally, the ejected water was as hot as coffee according to local people, when the fill of Navlakhi Harbour liquefied (Fig. 17.12) during the 2001 Gujarat earthquake of India (Towhata et al. 2002).

Fig. 18.14 Explosion to trigger liquefaction

Fig. 18.15 Field shaking test for verification of drain pipe technology

In contrast to those *hot* events in Turkey, Iran, India, and the Philippines, no such event has been known in Taiwan, Japan, and California. When Mr. F. Yuminamochi was taking a motion picture of boiling water in Niigata (Fig. 25.59) in June, 1964, he never felt anything warm although his feet were under ejected water. No shaking model test and cyclic undrained tests reported warm liquefaction. The only one exception is Jouanna et al. (2000) who elevated the ground temperature by merely 2°C after artificially shaking ground for 1 h at 10 Hz with the acceleration level of 200 Gal.

To throw light on this topic, the author measured the temperature of boiled water when artificial liquefaction was generated by subsurface explosion at Tokachi Harbour, Nov. 2001 (Port and Harbour Research Institute; Fig. 18.14). Prior to the test, the air and ground water temperatures were 10 and 3.8 °C, respectively. After shaking, the temperature in the ejected water ranged from 4–10 °C. Similarly, in-situ liquefaction tests were carried out by the Zenitaka Corporation using mechanical shaking (Fig. 18.15). The temperature of the ejected water was 16°C, while the air and ground water temperatures prior to shaking were 9 and 16°C. Thus, no hot liquefaction was detected. It seems quite likely that the hot liquefied water in the past was made hot by surface soil that was heated by sunshine in the daytime and through which pore water was ejected at the time of liquefaction.

18.7 Undrained Shear Tests of Sand

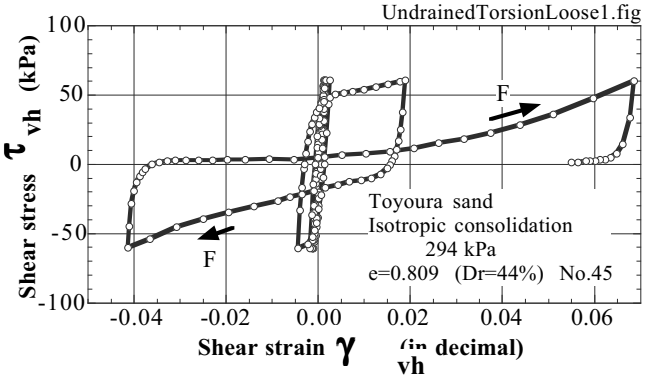

Fig. 18.16 Undrained stress–strain behavior of loose sand

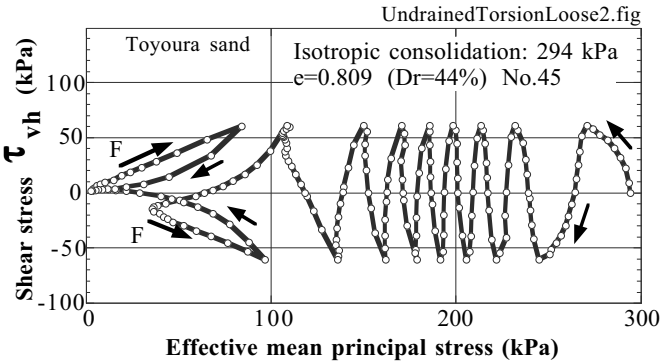

Fig. 18.17 Stress path of loose sand

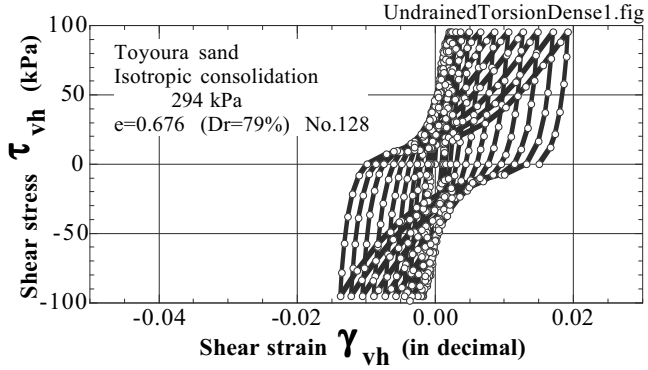

Fig. 18.18 Undrained stress–strain behavior of dense sand

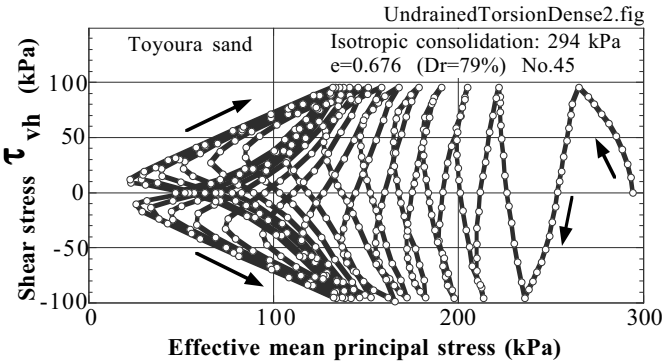

Fig. 18.19 Stress path of dense sand

Figures 18.16 and 18.17 illustrate the stress–strain and the stress-path diagrams of loose Toyoura sand. A hollow-cylindrical specimen was isotropically consolidated and then sheared by a torsion shear apparatus (Set. 18.8). It is seen that

1. The strain amplitude starts to increase drastically after some number of loading cycles
2. This strain increase seems to be associated with 50% pore pressure rise (excess pore water pressure = 50% of initial effective stress)
3. After 50% pore pressure rise, a few cycles of loading is sufficient to induce large deformation and zero effective stress (liquefaction)
4. In the final stage (shown by "F" in Fig. 18.17), the effective stress state moves along the failure line (dilative behavior), increasing effective stress as shear stress is loaded
5. In the meantime, the tangent modulus increases due to the increased effective stress (Fig. 18.16)
6. In the final stage of loading, pore pressure increases during unloading shear stress, while pore pressure drops in the course of loading [as stated in 3]; opposite from what was observed in early stages

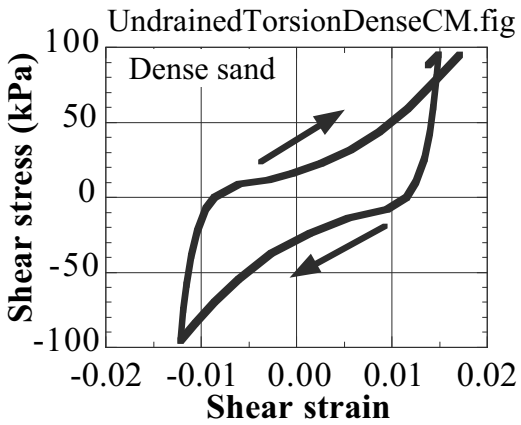

Fig. 18.20 Cyclic mobility

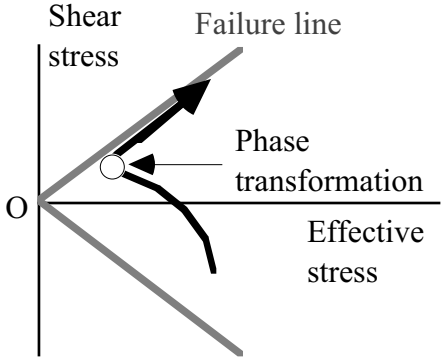

Fig. 18.21 Phase transformation in undraiend stress path of sand

Figures 18.18 and 18.19 show similar test results obtained from dense Toyoura sand. The shear strain does not increase so rapidly as in Fig. 18.16. One part of the stress strain curve is depicted in Fig. 18.20. The slope (tangent modulus) increases as the shear stress is loaded because of increasing effective stress (Fig. 18.19 and Fig. 18.21). This behavior is called cyclic mobility and prevents development of large shear strain. Moreover, the effective stress does not reach zero. Thus, dense and compacted sand has a good resistance against liquefaction. Therefore, densification of sand (compaction) is the most important remedial measure 対策 against liquefaction (Sect. 26.4). It is good that the effect of densification is permanent without maintenance. Dense sand is unlikely to liquefy because its void ratio is close to the minimum void ratio (e_{min} in Sect. 1.2) and there is not much volume contraction any more.

The transition from contractive behavior to dilatant one (decreasing effective stress to increasing) is called phase transformation (Fig. 18.21).

18.8 Torsion Shear Device with Hollow Cylindrical Specimen

In spite of its convenience,the triaxial shear device (Sect. 1.9) has several limitations. For example,

- It has only two independent stress components, while reality has three components in two-dimensional situation or six in three-dimensional conditions
- The orientations of principal stress axes (σ_v and σ_h) are fixed in vertical and horizontal directions, whereas those axes rotate in real loading conditions

These limitations have been overcome by a torsion shear device that tests a hollow cylindrical specimen (Fig. 18.22). Similar to a conventional triaxial machine, this torsion shear device shears a specimen that is covered by rubber membranes and consolidated under cell water pressure (Fig. 18.23). Since the outer and inner cell pressures in the horizontal direction are equal in many cases, there are three degrees of freedom in stress control (σ_v, σ_h, and τ_{vh} in Fig. 18.22), and the radial and tangentially horizontal stresses are considered equal to each other ($=\sigma_h$). Consequently, the effective mean principal stress, P', is defined by

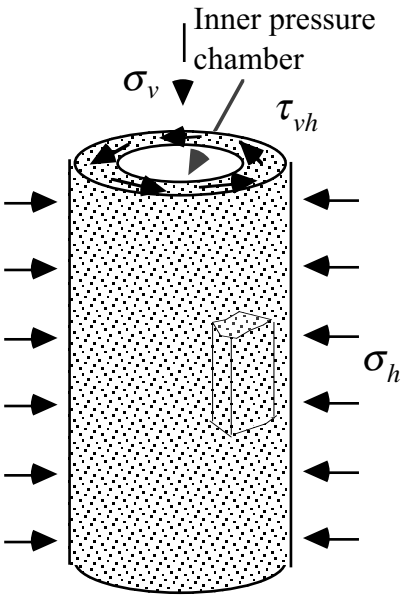

Fig. 18.22 Stress application on hollow cylindrical specimen

$$P' = (\sigma_1' + \sigma_2' + \sigma_3')/3 = (\sigma_v' + 2\sigma_h')/3 \qquad (18.4)$$

These components of stress are loaded on a hollow cylindrical specimen and the field stress condition is reproduced. Many tests have been conducted on liquefaction problems by using this apparatus.

The orientation of the major principal stress axes measured from the vertical direction (Fig. 18.24) is given by

$$\beta = \left\{\arctan\left(\frac{2\tau_{vh}}{\sigma_v - \sigma_h}\right)\right\} \Big/ 2. \qquad (18.5)$$

Fig. 18.23 Hollow cylindrical specimen undergoing consolidation (by G. Arangelovski)

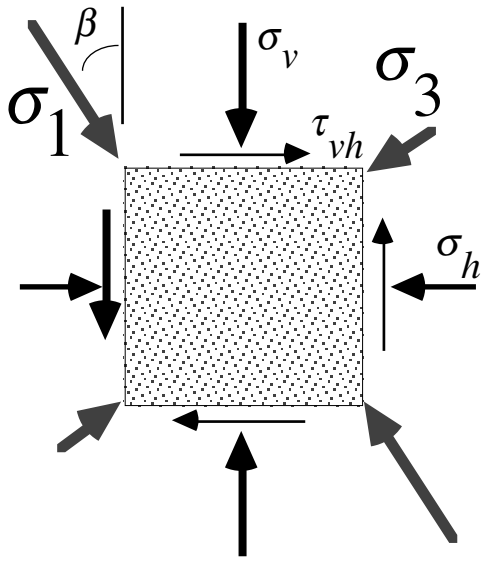

Fig. 18.24 Definition of orientation of major principal stress

Another advantage of this device is that there is no end in the peripheral direction. Therefore, this device avoids the problem of nonuniform stress that is caused by end effects.

When undrained shear is conducted with lateral confinement (zero lateral strain) in the radial direction, the drainage valve of a specimen and another water inlet to the inner cell that is completely filled with water (see Fig. 18.22) are closed. This situation is equivalent with cyclic loading of level ground undergoing K_o condition.

It is sometimes stated that the torsion shear device cannot test an undisturbed soil specimen. It is not correct, actually. When the outer diameter of a tested specimen is 10 cm, a large undisturbed sample of at least 10 cm in diameter is trimmed to a hollow cylindrical shape so that it fits the employed size.

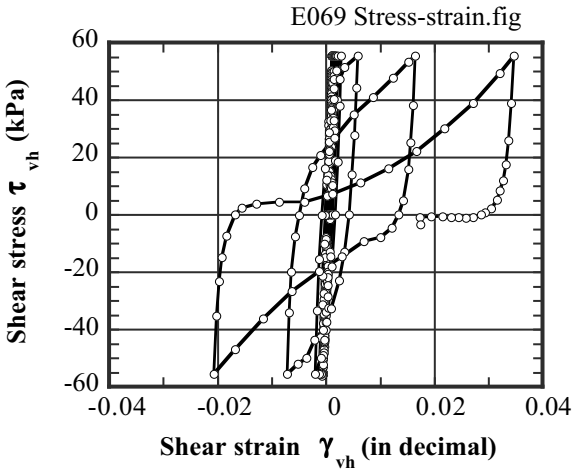

Fig. 18.25 Stress–strain diagram in cyclic undrained torsion shear test

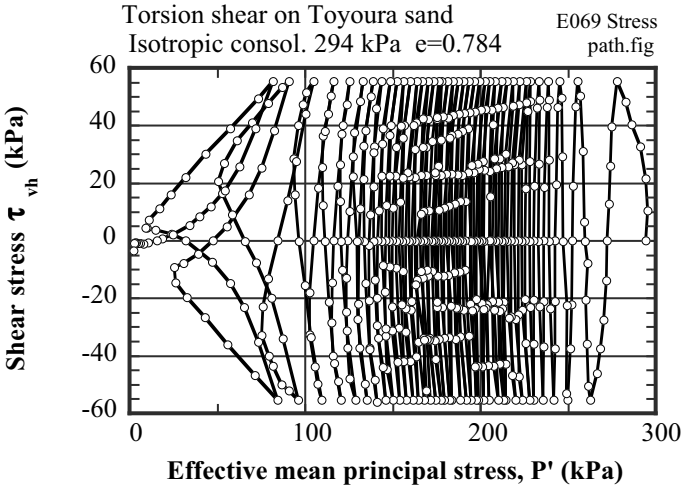

Fig. 18.26 Stress-path diagram in cyclic undrained torsion shear test

An attempt has been made to increase the degree of stress freedom to four by applying different horizontal pressures in inner and outer chambers. This measure generates different horizontal stress in the radial and circumferential directions of a specimen. Although this is an attractive idea, care should be taken of heterogeneity of stress. The different horizontal pressures vary the radial stress in the specimen from its inner face to the outer face.

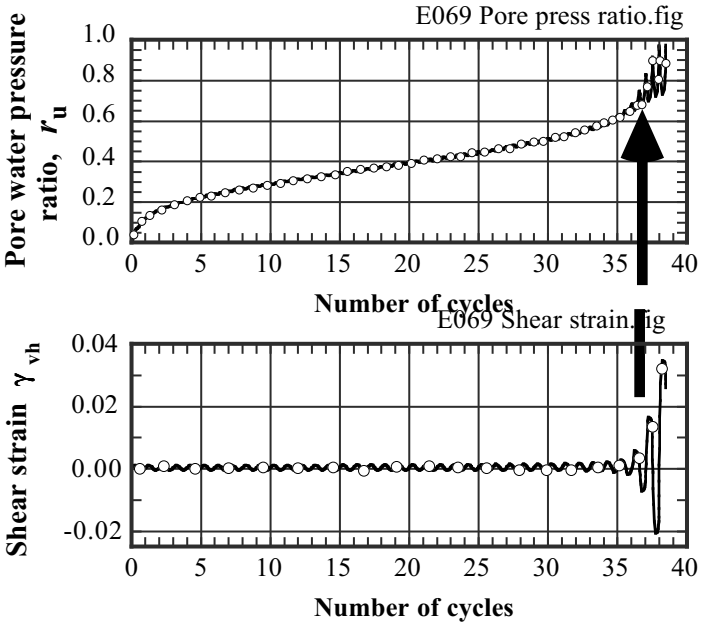

Fig. 18.27 Comparison of pore pressure ratio and shear strain amplitude in undrained cyclic torsion shear

Similar to Figures in Sect. 18.7, Figs. 18.25 and 18.26 present undrained cyclic shear data. The number of cycles here is much greater than those in Sect. 18.7. This set of data was replotted in Fig. 18.27 where the variation of excess pore water pressure ratio (r_u = excess pore water pressure / initial consolidation stress) is compared with the variation of shear strain amplitude. It is seen that sand becomes significantly soft and the shear strain amplitude starts to increase when the pore water pressure development exceeds approximately 60% of the initial consolidation pressure.

18.9 Effects of Subsurface Liquefaction on Intensity of Acceleration Response at Surface

The seismic isolation technology of modern buildings employs a very soft material in the foundation to avoid strong base-shear force that generates high acceleration in the super structure. The same principle holds true in a liquefied deposit where shear modulus is reduced drastically and high shear stress is not transmitted to the ground surface. This phenomenon is interpreted by the Newtonian equation of motion;

Acceleration at surface = Shear stress in liquefied subsoil /Mass of surface soil.

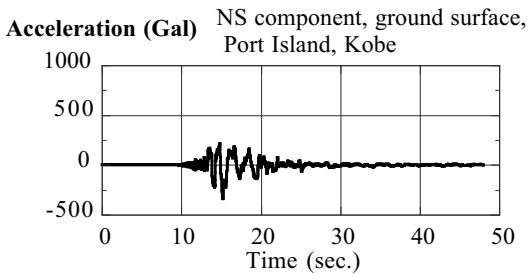

Fig. 18.28 Acceleration record at surface of Port Island

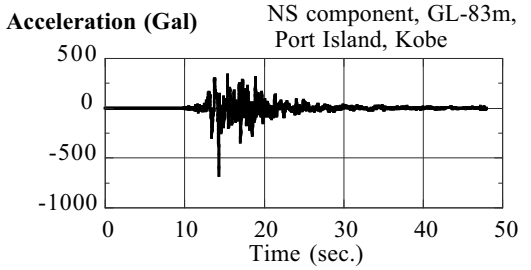

Fig. 18.29 Acceleration record at GL-83m of Port Island

Figures 18.28 and 18.29 compare the acceleration time histories in the NS direction which was recorded in Port Island of Kobe in 1995 by a seismic vertical array deployed by the Development Bureau of Kobe City Government. It is evident that the maximum acceleration at the surface was weaker than the one at the depth of 83 m far below the liquefied deposit. It is important as well that the surface acceleration had a longer predominant period than the bottom motion, which is the consequence of softening of liquefied subsoil and the elongation of the natural period (resonance). Accordingly, Fig. 18.30 shows the variation of maximum acceleration in all the three directions. The reduction of accelerations in the top 20 m is evident. The assessment by SI (Set. 23.4) suggests that the same range of soil liquefied; *MASA* soil that is a decomposed granite used for reclamation in 1960s and 1970s.

The elongated shaking period in Fig. 18.28 affected the velocity and displacement responses in Figs. 18.31 and 18.32. After time integration, the surface response became "greater" than the subsurface ones. Thus, although the reduced acceleration is probably less hazardous for superstructures above the surface, the increased displacement is hazardous to embedded lifelines and other facilities that are vulnerable to displacement-induced damages.

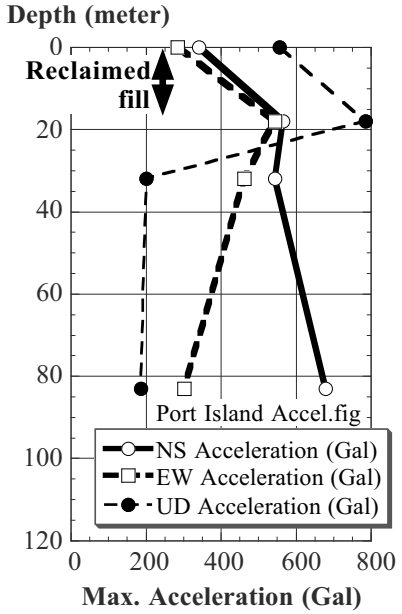

Fig. 18.30 Variation of maximum acceleration with depth in Port Island

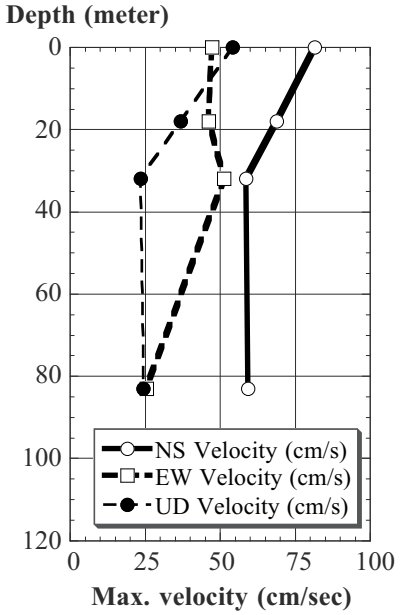

Fig. 18.31 Variation of maximum velocity with depth in Port Island

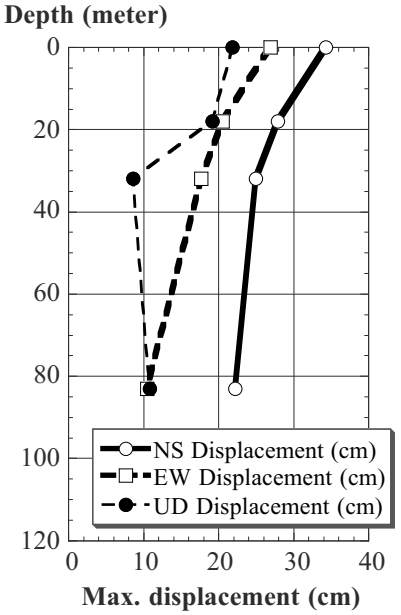

Fig. 18.32 Variation of displacement amplitude with depth in Port Island

18.10 Consolidation after Liquefaction

The bilinear distribution of excess pore water pressure during dissipation/consolidation (Sect. 18.3) means that the critical hydraulic gradient continues for a long time near the surface until dissipation is completed. It is noteworthy that the conventional theory of consolidation by Terzaghi cannot predict such a bilinear pore pressure distribution. Therefore, a numerical analysis on the procedure of pore-pressure dissipation after liquefaction, as is often conducted for design of gravel drain (Sect. 26.11), should not employ Terzaghi theory.

It is important that the volume change behavior of liquefied sand during dissipation of pore pressure is different from what Terzaghi theory assumes. Terzaghi theory employs a constant value of volume compressibility, m_v, which supposes a linear relationship between effective stress and volume change. Liquefied sand, conversely, does not exhibit such a linear behavior.

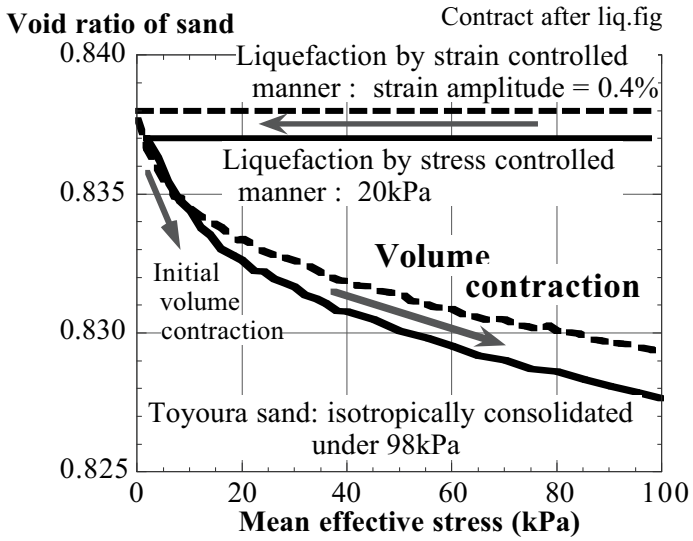

Fig. 18.33 Volume contraction of Toyoura sand after liquefaction

Figure 18.33 illustrates the variation of effective stress and void ratio of Toyoura sand specimen during undrained cyclic loading and the following dissipation/consolidation. Errors due to membrane penetration (Sect. 1.9) was corrected for by using the method by Sivathayalan and Vaid (1998). Liquefaction was induced by two manners, namely stress-controlled (constant stress amplitude) and strain-controlled (constant strain amplitude) manners. When effective stress started to increase again due to reconsolidation, void ratio did not respond in a linear way. As shown in Fig. 18.33, the stage of initial volume contraction (Fig. 18.33) generated greater volume compressibility than in the following stages. This suggests that sand grains that are floating in pore water during 100% liquefaction (Sect. 18.1) deposit quickly in the first stage of effective stress increase.

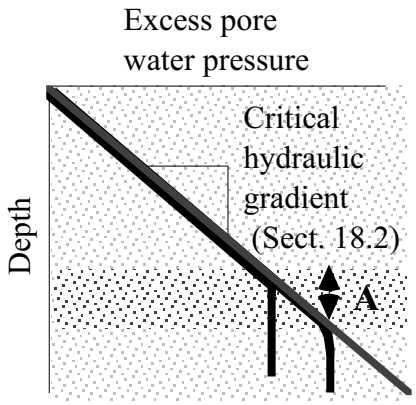

Fig. 18.34 Bilinear distribution of excess pore water pressure during dissipation and reconsolidation

From the viewpoint of seepage flow, the substantial amount of pore water that is drained out from the lower layer (initial volume contraction in layer **A**, Fig. 18.34) is used to maintain high pore water pressure and the critical hydraulic gradient in the upper layers. In conclusion, it is necessary to take into account the large volume compressibility of sand undergoing the initial volume contraction to make a reasonable prediction of excess pore water pressure change during its dissipation process.

18.11 Liquefaction Potential and Surface Geology

The possibility of liquefaction (liquefaction potential) is high in loose deposits of sand. In contrast, liquefaction is unlikely in dense sandy deposits. Liquefaction is not possible when there is no ground water. In a gigantic slope failure, furthermore, pore air may play the same role as pore water in liquefaction;

effective stress = total stress – pore air pressure → zero.

Figure 17.8 demonstrated that the Shinano River in Niigata City was wider in previous times, and the area that was reclaimed in the twentieth century (Kawagishi-Cho) developed substantial liquefaction in 1964 (Fig. 17.6). Figure 18.35 is a map of Niigata City, which was published in early twentieth century. The Shinano River is drawn in the center. This river channel was twice wider in those days. By the middle of twentieth century, two flood channels were constructed in the upstream area, directly connecting this river and the sea, and it thereby became possible to reduce the river width in Niigata City for urban development. The land reclamation project was carried out by transporting fine uniform sand from the dune along the beach and throwing sand into the big inlet of the river. No densification was undertaken because sand was considered to be a good foundation soil (without consolidation settlement) in those days. Consequently, loose water-saturated young deposit of sand was formed. This is the place where liquefaction occurred intensely and apartment buildings tilted or fell down in 1964 (Fig. 17.6). Dagupan City of the Philippines where liquefaction occurred substantially in 1990 (Sect. 17.5) has a similar history of development; in the middle of the twentieth century, rice fields and fish ponds were reclaimed by throwing beach sand into water (Fig. 18.36). No liquefaction occurred in older ground of the city (Fig. 18.41).

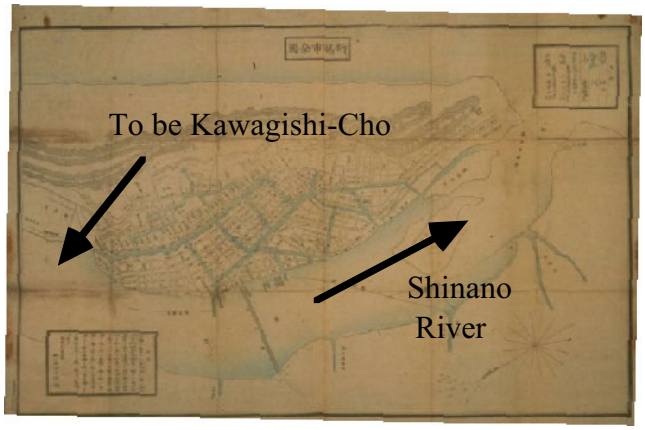

Fig. 18.35 Niigata City in early twentieth century

Fig. 18.36 Waters in Dagupan City

Loose sandy deposit with high ground water table is found in the following geological settings.

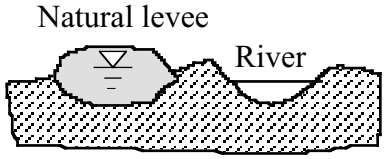

Fig. 18.37 Natural levee

Land reclamation 埋立地: sedimentation in water makes loose sand packing (relative density being around 40%), young age of sand means no significant cementation, and few experience of strong earthquake shaking.

Abandoned river channels 旧河道: abandoned channels are often filled with natural sand deposit that is not compacted naturally.

Low land between sand dunes and near edge of dune hill 砂丘間低地 : Dune sand has good resistance against liquefaction because it is dense due to wind action and water table is low. However, dune sand is transported downwards and deposits softly in low places where there is normally much water

Minor natural levee 自然堤防 : flooding leaves a natural embankment of sandy materials (Fig. 18.37); a natural levee itself is dry and good to live, but ground water table is high and sand may not be dense.

Liquefaction is not possible in terrace, hill, and mountains where neither loose young deposit of sand nor ground water is there. Those liquefaction-vulnerable soil conditions are usually accompanied by low SPT-*N* and cone penetration resistance.

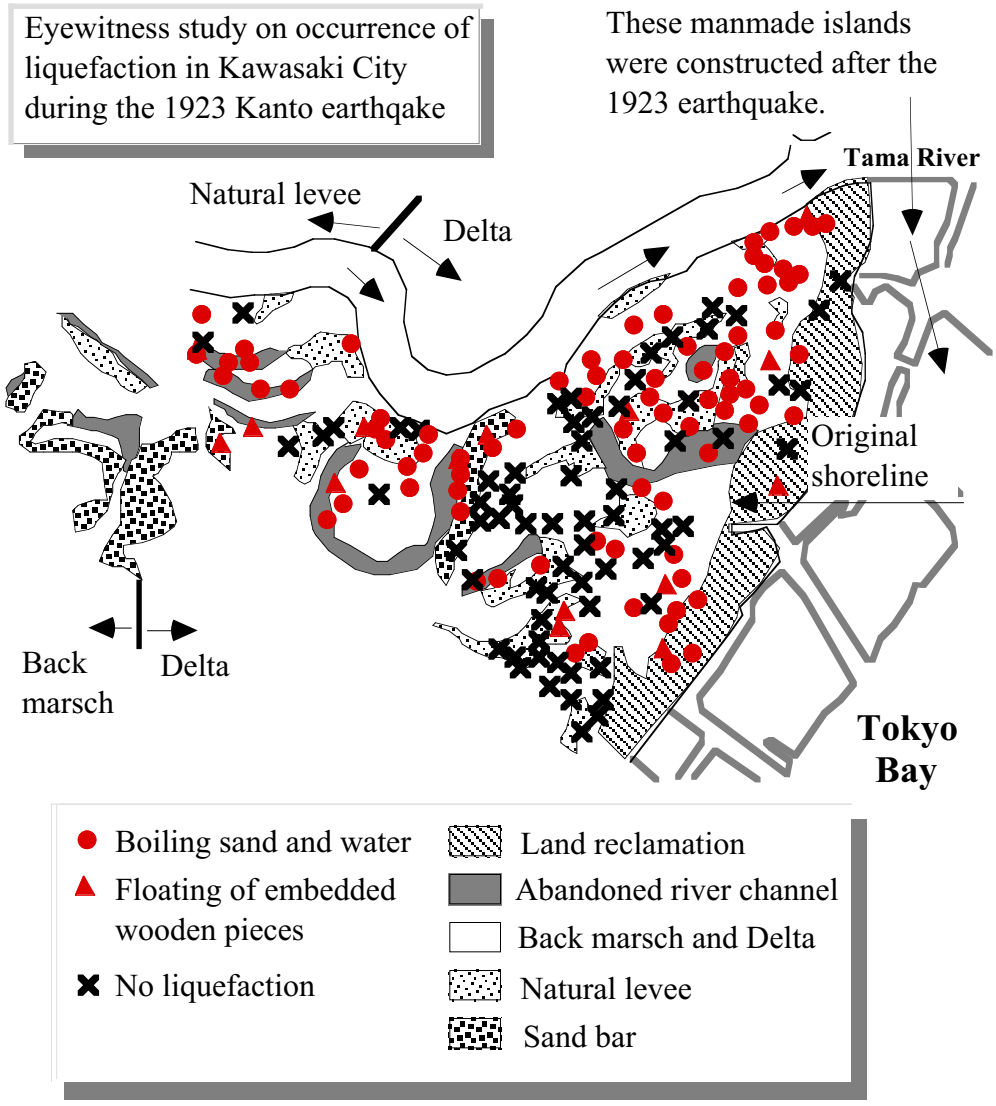

Fig. 18.38 Sites of liquefaction in Kawasaki, 1923 (Kubo et al. 1979)

Figure 18.38 is a case history study of liquefaction in the Kawasaki City during the Kanto earthquake in 1923. When an eyewitness mentions boiling of sand or floating of embedded wooden objects, it is judged that liquefaction occurred at the particular place. Note that area without any symbol in Fig. 18.38 may have developed liquefaction; missing of symbols simply means that there is no eyewitness.

Liquefaction mostly occurred along the abandoned channels of the Tama River and in its alluvial plain. The marine reclamation was not there in 1923. On the contrary, it is empirically known that beach sand has higher liquefaction resistance probably because it was densified by cyclic wave action.

Wakamatsu (1991) compiled an enormous amount of documents and eye-witness reports, which were mostly collected by herself, to identify the location of sand boiling and other liquefaction evidences all over Japan during past earthquakes. It is very useful to learn from her achievements that abandoned river channel is highly vulnerable to liquefaction.

18.12 Maximum Distance of Liquefaction Sites from Source Area

It is important from the perspective of seismic hazard assessment to predict the size of area where liquefaction is quite likely to occur. Basic data for this was assembled by using documented liquefaction during past earthquakes. Since people in old days did not use the term of "liquefaction," alternative expressions such as boiling of sand and water, ejection, surface depression, subsidence of buildings, floating of embedded structures and likes had to be detected in literatures and interpreted.

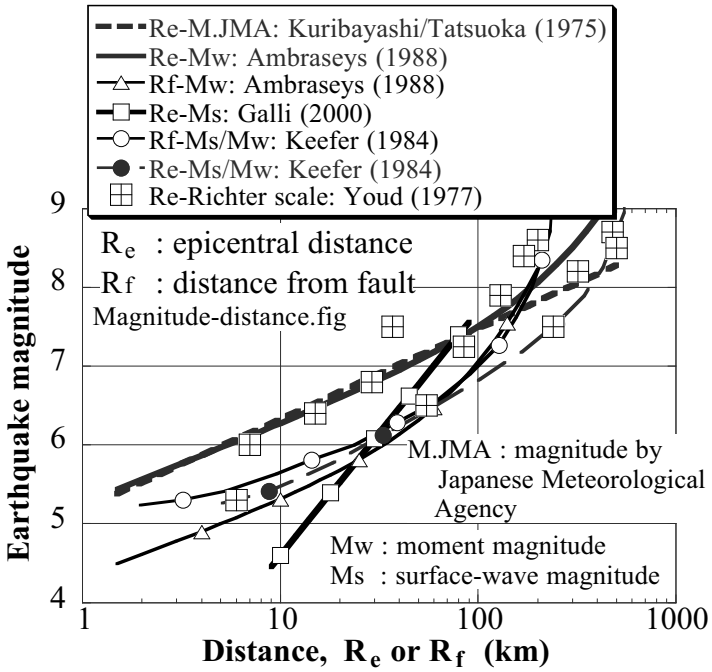

Fig. 18.39 Maximum distance to liquefaction sites varying with seismic magnitude

Kuribayashi and Tatsuoka (1975) collected informations in Japanese earthquakes and did this job. The upper bound of the epicentral distance, R_e (Set. 5.10), at sites of liquefaction was taken for respective seismic magnitude. Since no magnitude of modern sense was known for historical earthquakes, the Kawasumi magnitude (Set. 5.4), which relies on the documented extents of damage, was used in place of M_{JMA} (magnitude determined by the Japanese Meteorological Agency in Set. 5.4). Consequently,

$$\log_{10}(R_e) = 0.77 M_{JMA} - 3.6 \tag{18.6}$$

was derived; the unit of the epicentral distance, R_e, is kilometer. Ambraseys (1988) stated that Kuribayashi reduced the assessed Kawasumi magnitude by *0.5* for historical earthquakes before 1922. Accordingly, a revised formula was proposed;

$$\log_{10}(R_e) = 0.88 M_{JMA} - 4.4 \tag{18.7}$$

Afterwards, several studies of a similar type have been performed by using case histories in different parts of the world. For example, Ambraseys (1988) obtained

$$\begin{aligned} M_w &= -0.31 + 2.65 \times 10^{-8} R_e + 0.99 \log_{10}(R_e) \\ M_w &= 0.18 + 9.2 \times 10^{-8} R_e + 0.90 \log_{10}(R_f) \end{aligned} \tag{18.8}$$

in which R_e and R_f (distance from fault) are given in "cm" unit. Moreover, Galli (2000) obtained

$$M_s = 1.5 + 3.1 \times \log_{10}(R_e) \tag{18.9}$$

where R_e is in *km* unit. In summarizing liquefaction-induced soil flow, Keefer (1984) used M_s when it is less than *7.5* and M_w when it is greater than *7.5*. Youd (1977) added data from many parts of the world. Although not clearly mentioned, his magnitude is probably the Richter magnitude. All the empirical formulae and data as mentioned earlier are summarized in Fig. 18.39. Note that liquefaction at the greatest distance is likely to be associated with the most liquefaction-prone soil conditions such as very loose young sandy deposit, amplification of motion by basin structure (Sect. 5.8) etc.

18.13 Effects of Ageing on Liquefaction Strength of Fill

Figure 17.34 indicated the totally different behaviors of ground in Dagupan City, the Philippines. Although the younger ground subsided upon the 1990 Luzon earthquake due to liquefaction, the older natural-levee ground did not. A similar contrast is found between Figs. 18.40 and 18.41. While the former illustrates subsidence of building into liquefied ground, the latter shows the situation in the area of natural levee where no liquefaction occurred. Dagupan City was founded in this area by the Spanish people, and was expanded to the water area of rice field and fish pond in the twentieth century (Sect. 18.11). The new city area was made by placing beach sand in water, resulting thus in young loose water-saturated ground, which is highly vulnerable to liquefaction.

Fig. 18.40 Subsidence of building in Dagupan City due to liquefaction

Fig. 18.41 Area without liquefaction in Dagupan City

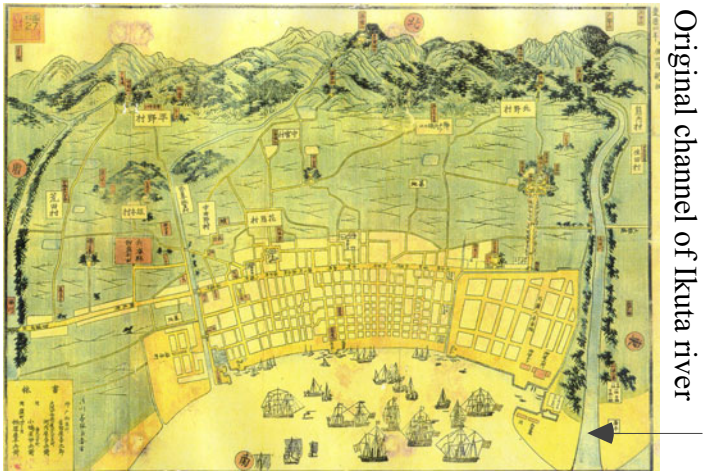

Fig. 18.42 Kobe Harbor in 1868

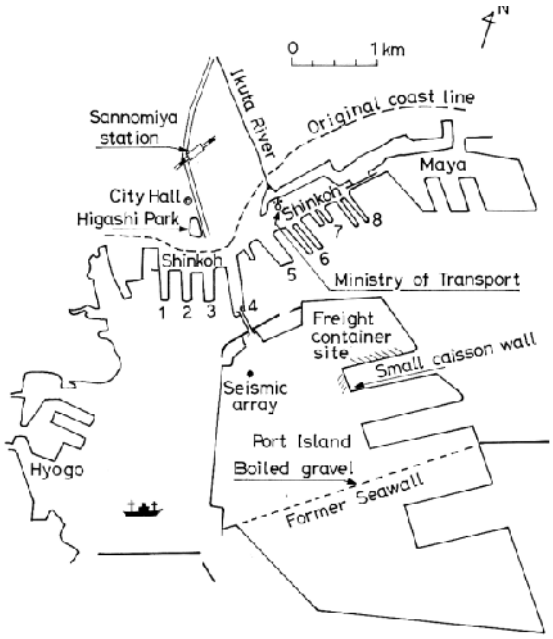

Fig. 18.43 Location of liquefaction in coastal area of Kobe, 1995

Kobe harbor was constructed by filling soil in the sea. Figure 18.42 indicates the Kobe Harbor in 1868 before modern harbor construction was initiated. Figure 18.43 shows the area of Kobe Harbor in 1995. It is seen therein that Port Island, which suffered significant liquefaction, (Sects. 17.8, 20.2, 26.1) is located to the south of the original coast line. It means that liquefaction was substantial in young reclamation. In contrast, to the north of the original coast line, only very minor liquefaction was seen; for example in the Higashi Park as shown in Fig. 18.44. A similar contrast in liquefaction resistance was found in the coastal area of Nishinomiya, which is located to the east of Kobe. Figure 18.45 shows that no liquefaction occurred to the right hand side of an original sea wall because the soil condition here was a natural and aged sand. Conversely, beyond the sea wall, the subsoil was a product of very recent (after 1970) reclamation and liquefaction occurred significantly.

Fig. 18.44 Minor liquefaction in Higashi Park on inland side of original coast line in Kobe

Fig. 18.45 Contrast in liquefaction resistance due to age difference

Thus, there is a significant difference in possibility of liquefaction due to the age of soil. Although volume compression after liquefaction (Sect. 18.10) increases the density of sand, its resistance against liquefaction does not increase so much as may be expected; see repeated liquefaction in Sect. 22.2.

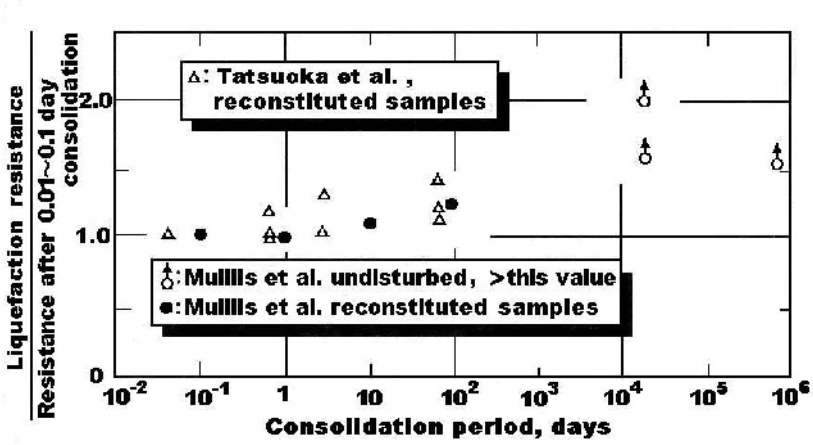

Fig. 18.46 Effects of consolidation time on liquefaction resistance

Most probably the liquefaction resistance of sand is increased by age. Although the details of ageing effects are not yet known, the first issue may be the accumulated densification effects because of historically repeated strong earthquakes. For example, Japanese sandy ground that is probably a few thousand years old hardly liquefies because of active seismicity, while aged pleistocene sand in the New Madrid area, Central USA, liquefied during the 1811–1812 New Madrid earthquake. Probably, low seismic activity in this area did not densify natural sand and liquefaction resistance was still low.

The ageing effects have been reported from laboratory tests as well (Fig. 18.46). In this figure, the data by Tatsuoka et al. (1988) comes from laboratory shear tests, which show that sand after longer consolidation has greater resistance, although no earthquake loading occurred to the specimen. Mulilis et al. (1977) compared laboratory measured strength against assessed behavior of aged sand to show the increase of strength with age. Moreover, Seki et al. (1992) collected undisturbed sand samples from a site in Kamakura where sand boil evidences the liquefaction (Sect. 18.2) 700 years ago. The cyclic triaxial tests on undisturbed and laboratory-reconstituted specimens revealed that the undisturbed samples, which

were 700 years old since the previous earthquake, is 1.3–1.4 times more resistant. Note that the relative density of the undisturbed samples were 73–82%, while the reconstituted samples were looser (67–72%).

Finally, Fig. 18.47 illustrates the effects of minor cyclic (drained) shear (prestraining) on liquefaction resistance of sand of medium density. The prestraining was intended to reproduce effects of minor past earthquakes. Although prestraining with the stress ratio of 0.25 with 100 cycles induced only 0.3% of volumetric contraction, the increase in the liquefaction resistance was remarkable. In summary, it seems that ageing is induced by two agents: repeated compaction due to minor earthquakes and grains dropping into big voids (Sect. 1.14).

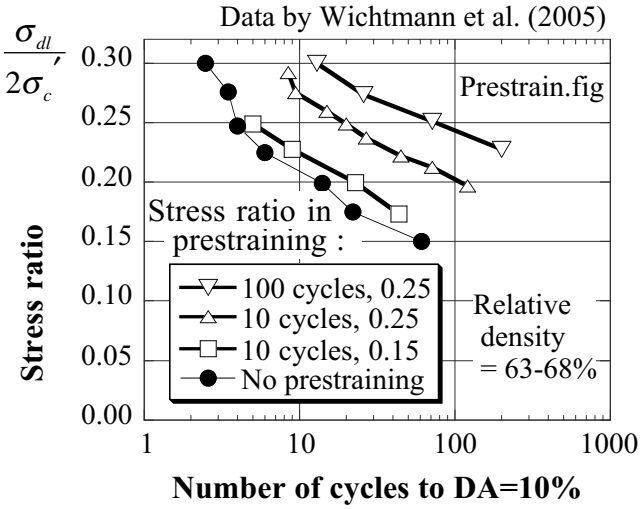

Fig. 18.47 Effects of prestraining on liquefaction resistance of sand (data by Wichtmann et al. 2005)

It seems that these findings on ageing suggests very low potential of liquefaction in natural deposits of sand that are at least hundreds of years old and have experienced several strong earthquakes. Possibly repeated liquefaction (Sect. 22.2) finally results in sufficiently high density and resistance of sand and also minor shaking generates the prestraining effects. This idea is consistent with the empirical knowledge that most significant liquefaction has occurred in young artificial deposits or backfill of sand (Chap. 17). It may be, therefore, said that liquefaction risk in sea bed is high only in special environments where the rate of sedimentations is very high, for example, near a mouth of a big river (Fraser River mouth in Chillarige et al. 1997; Valdez Harbor in Fig. 15.52). In contrast, the submarine ground in a continental shelf where the rate of sedimentation is, for example, 0.1 cm/y or less (Saito, 1993) is not susceptible to liquefaction except in the top 1 m. This suggests that a destructive lateral flow of liquefied soil (Chap. 24) is quite unlikely in sea bed except in a special environment such as that off a river mouth. This idea is beneficial to submarine development in seismically active region of the world, although further geological evidence and soil investigation, such as submarine CPT, are needed.

18.14 Liquefaction in Natural Deposit of Loose Sand

Section 18.13 revealed that liquefaction in older natural deposits is less likely than in recent artificial fill. The experience in Kobe, 1995, agrees with this idea. The Kawagishi-cho site in Niigata was filled artificially by using clean sand in about 1930 (Fig. 18.35). The Marina district in San Francisco where liquefaction occurred in 1989 Loma Prieta earthquake was filled in 1900s. The liquefaction in fill of Dagupan City is in line with these experiences. The good resistance of natural and more aged sandy deposit against liquefaction comes probably from the ageing (Sect. 18.13), the densification by repeated shaking during past earthquakes, and possibly another densification by wave action.

Fig. 18.48 Map of the Luzon Island, the Philippines

The heavy liquefaction in the Narbakan Village (Fig. 17.30) occurred in a natural deposit of sand. This may appear exceptional. Figure 18.48 shows the Luzon Island of the Philippines in which the Lingayen Gulf is seen on the north-west part of the Island. The Narbakan village is located on a small sandy peninsula to the north of Dagupan. The important feature of this sandy subsoil is the rapid sedimentation of sand. Figure 18.49 was taken around 1940 of the peninsula. The rapid growth of the peninsula in consequence of sedimentation is evidenced by the laminar structure of the surface. Inside the inland sea between the peninsula and the mainland (Fig. 18.50) there is only weak wave action, which exerts limited cyclic loading and densification. The young sandy deposit without sufficient ageing had not experienced seismic densification in the past. Consequently, the sand in the peninsula had low resistance against liquefaction at the time of the earthquake in 1990.

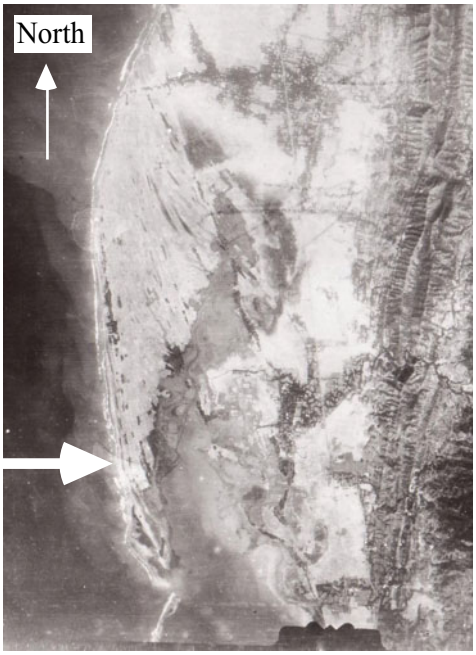

Fig. 18.49 Narbakan peninsula in air photo (National Archives, Washington D.C.)

Fig. 18.50 Inland sea between mainland and peninsula of Narbakan

18.15 Significance of Cyclic Triaxial Tests in Liquefaction Problems

Although shaking model tests can provide important information about mechanism of liquefaction, it cannot assess the liquefaction potential of specified sites. This assessment is done by running cyclic triaxial tests on undisturbed soil samples (Sect. 10.19) collected at sites.

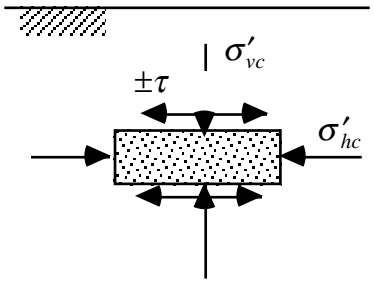

Fig. 18.51 Seismic stress state in level ground

Figure 18.51 illustrates an idealized stress state during earthquakes in a level ground. Prior to earthquakes, the effective stress has a K_o state ($\sigma'_{hc} = K_0\sigma'_{vc}$; anisotropic consolidation; 異方圧密) and there is no shear stress in the horizontal plane. The vertical propagation of *S* wave produces in the horizontal plane a cyclic shear stress, which alternates in positive and negative directions and induces negative dilatancy of sand fabric (砂の粒子構造) as well as build-up of excess pore water pressure. The amplitude of the cyclic shear stress is denoted by τ. Although there is a need to reproduce this stress state in a laboratory, an appropriate testing machine (cyclic simple shear or torsion shear device) is not widely available. More important is that a soil specimen of rectangular (直方体) or hollow cylindrical (中空円筒) shape, which is required by those testing machines, does not suit the use of undisturbed soil specimens collected by insitu soil samplers.

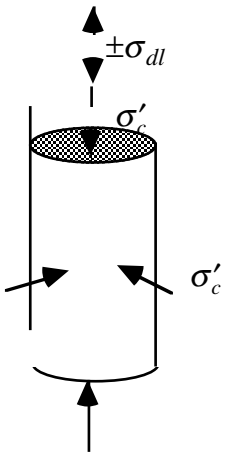

Fig. 18.52 Stress state in cyclic triaxial tests

Consequently, cyclic triaxial testing on *undisturbed soil samples* (Sects. 10.17 and 10.19) is widely practiced. Figure 18.52 indicates the stress state in this testing. A soil specimen is isotropically consolidated under the effective stress of σ'_c, which is normally set equal to the insitu effective vertical stress. After consolidation, a cyclic axial stress, $\pm\sigma_{dl}$, is loaded in undrained manners until large deformation occurs. Note that $\pm\tau$ in the horizontal plane in the field is replaced by $\pm\sigma_{dl}$ in the axial direction in the laboratory.

Stress states in Figs. 18.51 and 18.52 are different in the following points: (1) plane strain and axial symmetry, (2) anisotropic and isotropic consolidations, (3) rotation and fixed directions of principal stress, etc. Thus, perfect agreement between the field and the laboratory conditions is not possible. However, there is some similarity in stress states between Fig. 18.51 and the one in the 45° plane of a triaxial specimen (Fig. 18.53).

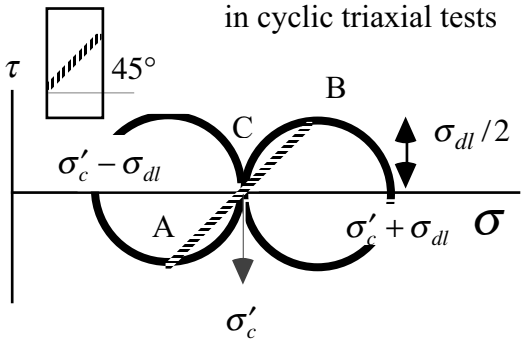

Fig. 18.53 Mohr´s stress circle during cyclic triaxial test

Figure 18.53 indicates a Mohr´s stress circle of a cyclically loaded triaxial specimen. The 45° plane is initially consolidated under σ'_c without initial shear stress (point C). Upon cyclic loading, its normal and shear stress vary in the range of $\sigma'_c \pm \sigma_{dl}/2$ and $\pm\sigma_{dl}/2$ (points A and B). Since the specimen is fully saturated with water, the variation of normal stress is 100% transferred to pore water pressure (Skempton´s B =1; Sect. 18.16), and does not affect the specimen. Thus, the normal stress variation is ignored and the following relation is found between the field and the laboratory; $\sigma'_{vc} \Leftrightarrow \sigma'_c$, $\pm\tau \Leftrightarrow \pm\sigma_{dl}/2$, and stress ratio $\tau/\sigma'_{vc} \Leftrightarrow \sigma_{dl}/(2\sigma'_c)$.

One may imagine that the normal stress upon the 45° plane can be maintained constant by varying both the axial stress by $\sigma_{dl}/2$ and the lateral cell pressure by $-\sigma_{dl}/2$. This is difficult in practice, because the cell pressure is controlled by pneumatic system (air pressure) that is slow in response and cannot operate in phase with the axial loading.

18.16 Skempton´s B Value

Cyclic triaxial tests on sand in the laboratory are performed by using water-saturated samples, because unsaturated sand is significantly less liquefiable than saturated insitu sand (Sect. 18.1).

The extent of water saturation of tested specimens is evaluated by using Skempton's *B* value. Skempton (1954) described the increment of pore water pressure in soil undergoing undrained stress increments by

$$\Delta u = B\{\Delta\sigma_3 + A(\Delta\sigma_1 - \Delta\sigma_3)\} \qquad (18.10)$$

where Δu is the increment of pore water pressure, while $\Delta\sigma_1$ and $\Delta\sigma_3$ are the increments of major and minor total principal stresses, respectively; they are not effective stresses. The first term in {} stands for the contribution by the isotropic stress increment, while the latter designates the component made by shear-induced dilatancy.

B is 1.0 when sand is ideally and fully saturated. Hence,

$$\Delta u = \Delta\sigma_3 \qquad (18.11)$$

when stress increment is isotropic ($\Delta\sigma_1 = \Delta\sigma_3$).

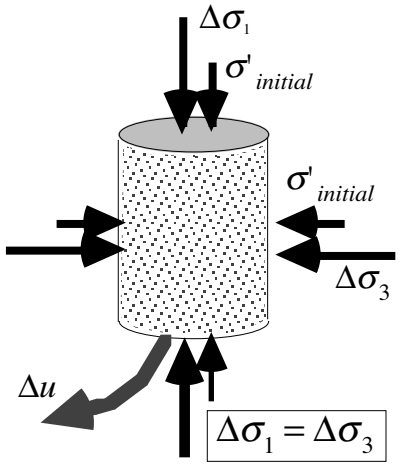

Fig. 18.54 Undrained isotropic loading of total stress for examining extent of saturation

In the practice of laboratory tests, the following procedure is made for good saturation.

1. A sand specimen is supported by low isotropic effective stress of σ'_{initial} in an assembled pressure chamber
2. To help achieve high extent of saturation, the pore air in the sample is removed either by using vacuum or circulating carbon-dioxide (CO_2) gas slowly through the specimen from its bottom to the top. Note that, when vacuum is employed, the applied external pressure has to be reduced as well so that the effective stress of σ'_{initial} may be maintained
3. De-aired water (distilled water without solved air) is then circulated slowly from the bottom to the top. The rate of circulation of gas and water has to be sufficiently slow; otherwise grain packing of sand would be disturbed by the flow
4. To examine the extent of saturation, the drainage valve of a triaxial device is closed and isotropic undrained compression is made; equal total stress increments are applied to the specimen; $\Delta\sigma_1 = \Delta\sigma_3$; see Fig. 18.54. The increment of pore water pressure, Δu, during this loading is measured
5. *The extent of saturation is evaluated by comparing the measured pore pressure increment with the theoretical value of fully saturated sand (18.11).*

$$B = \Delta u / \Delta\sigma_3 \qquad (18.12)$$

6. *B* greater than 0.95 (or 0.97, for example) is considered satisfactory. The water pressure in the pore water circuit of a testing machine is raised to the same level as the measured pore water pressure, the drainage valve is opened, and the consolidation stage is resumed
7. If saturation is not satisfactory, the drainage valve is opened in the same way as stated earlier, de-aired water is circulated again, and the *B* value is measured once more. Since the pore water pressure during this second attempt is higher than during the previous attempt, pore gas is solved in water, and improved saturation is very likely

Note that *B* value is still low even if the conventional degree of saturation, S_r, is close to 100%. Thus, the *B* value is a more sensitive index of saturation.

In shaking model tests on large deformation of liquefied slope (Chap. 23), it is possible that the recorded excess pore water pressure does not reach the initial effective stress level (what is called 100% development of excess pore water pressure), although the sand exhibits very soft behavior. While one of the reasons for this is the positive dilatancy and drop of pore water pressure due to large shear deformation (A<0), the other reason is the decrease of $\Delta\sigma_3$ (the disappearance of overburden pressure); $B\Delta\sigma_3 < 0$ at point P in Fig. 18.55. Because of the reduced overburden, the 100% development of excess pore water pressure is achieved under lower magnitude of pressure.

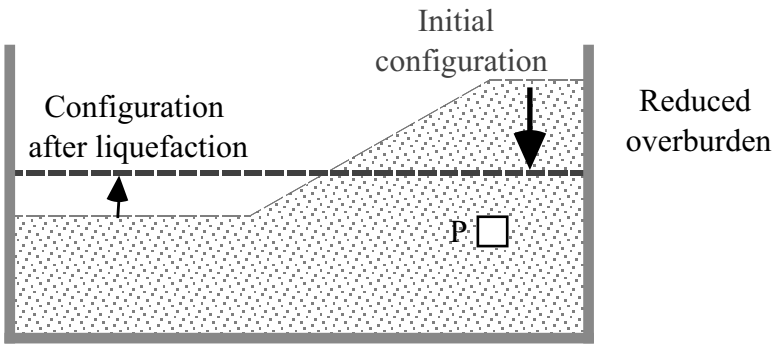

Fig. 18.55 Full development of liquefaction in model test at excess pore pressure lower than initial effective stress

18.17 Degree of Saturation and Skempton´s B Value

Since liquefiable subsoil is considered to be water-saturated, laboratory liquefaction tests make a lot of efforts to attain high extent of saturation in a specimen. The extent of saturation is evaluated by Skempton´s B value in place of the degree of saturation, S_r, because the B value is a more sensitive index when a specimen is near the complete saturation. The relationship between B value and S_r is going to be derived in this section.

Suppose an undrained isotropic loading of stress increment, $\Delta\sigma$, on a soil sample with pore water and minor amount of air bubbles (Fig. 18.56). The effective stress and pore water pressure increase by $\Delta\sigma'$ and Δu, respectively. The volume contraction of the soil skeleton (fabric of grains) is given by

$$\Delta\varepsilon_{\text{skeleton}} = m_v \Delta\sigma'$$

where m_v is the volume compressibility of soil skeleton (1.12).

The volume change of pore space is calculated by assembling contributions from pore water and pore air bubbles. The volume contraction of water is derived as

$$\Delta\varepsilon_{\text{water}} = \frac{eS_r}{1+e}\frac{\Delta u}{K_w}$$

in which "e" stands for the void ratio, $eS_r/(1+e)$ the volume of water per unit volume of soil, and K_w the bulk modulus of water.

When the effects of surface tension at the interface of water and air are ignored for simplicity, the pore air pressure increment is equal to that of pore water pressure, Δu. The volume of pore air changes from the initial value of $e(1-S_r)/(1+e)$ under the absolute pressure of P_a to a new volume of $e(1-S_r)/(1+e) - \Delta\varepsilon_{\text{air}}$ when the pressure increases from the absolute pressure of P_a to $P_a + \Delta u$. The absolute pressure starts from zero under perfect vacuum. Since the Boyle´s law states that *Pressure* × *Volume* is maintained constant,

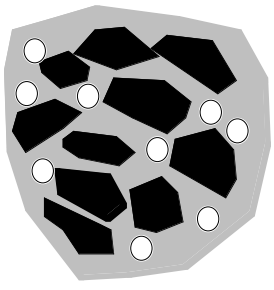

Fig. 18.56 Soil eloement consisting of particles, pore water, and air bubbles

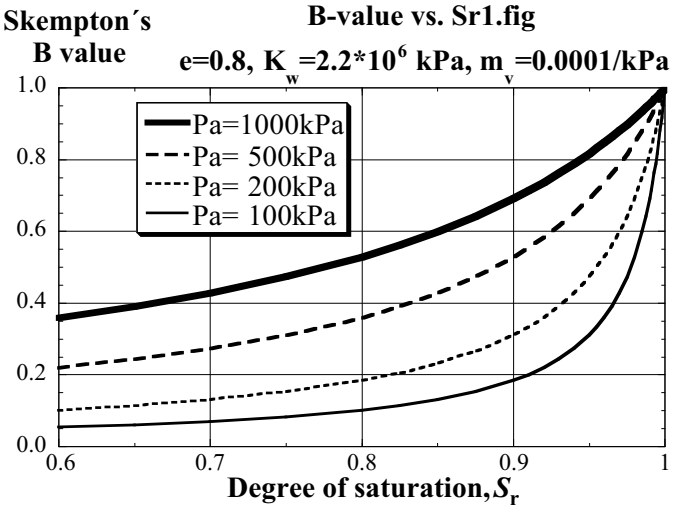

Fig. 18.57 Example calculation of Skempton´s B value varying with degree of saturation

$$P_{\mathrm{a}}\frac{e\left(1-S_{\mathrm{r}}\right)}{1+\mathrm{e}}=\left(P_{\mathrm{a}}+\Delta u\right)\left\{\frac{e\left(1-S_{\mathrm{r}}\right)}{1+e}-\Delta\varepsilon_{\mathrm{air}}\right\}$$

Accordingly,

$$\Delta\varepsilon_{\mathrm{air}}=\frac{e\left(1-S_{\mathrm{r}}\right)}{1+e}\frac{\Delta u}{P_{\mathrm{a}}+\Delta u}\approx\frac{e\left(1-S_{\mathrm{r}}\right)}{1+e}\frac{\Delta u}{P_{\mathrm{a}}}$$

when Δu is small. Note that solving of pore air into pore water is ignored.

No drainage is allowed upon undrained loading, and, therefore, the volume change of soil skeleton is equal to the volume change of pore;

$$\Delta\varepsilon_{\mathrm{skeleton}}=m_{\mathrm{v}}\Delta\sigma'=\Delta\varepsilon_{\mathrm{water}}+\Delta\varepsilon_{\mathrm{air}}$$

$$m_{\mathrm{v}}\left(\Delta\sigma-\Delta u\right)=\frac{eS_{\mathrm{r}}}{1+\mathrm{e}}\frac{\Delta u}{K_{\mathrm{w}}}+\frac{e\left(1-S_{\mathrm{r}}\right)}{1+e}\frac{\Delta u}{P_{\mathrm{a}}}=\frac{e}{1+e}\left(\frac{S_{\mathrm{r}}}{\mathrm{K_w}}+\frac{1-S_{\mathrm{r}}}{P_{\mathrm{a}}}\right)\Delta u$$

$$B\equiv\frac{\Delta u}{\Delta\sigma}=\frac{1}{1+\dfrac{e}{1+e}\left(\dfrac{S_{\mathrm{r}}}{\mathrm{K_w}}+\dfrac{1-S_{\mathrm{r}}}{P_{\mathrm{a}}}\right)\Big/m_{\mathrm{v}}}$$

Figure 18.57 illustrates an example calculation in which $e=0.8$, $K_{\mathrm{w}}=2.2\times10^{6}$ *kPa*, and $m_{\mathrm{v}}=10^{-4}$/kPa. The *B* value suddenly increases toward 1.0 when S_{r} exceeds 0.9. The minimum acceptable value of *B* in laboratory tests is *0.95–0.97*. When saturation is not satisfactory, the back pressure, P_{a}, is raised to higher values so that pore gas solves into water and the remaining size of bubbles is compressed and decreases further.

18.18 Effects of Sample Preparation Methods on Resistance to Liquefaction in Laboratory Shear Tests

The liquefaction resistance of insitu ground is evaluated by collecting undisturbed soil samples (Sects. 10.19 and 10.20) and running undrained cyclic shear tests. Although this measure is useful, different approach is needed for planning of earth fill dam and more basic studies on effects of a variety of soil properties on liquefaction phenomenon. If latter is the case, soil samples are prepared in a laboratory.

There are several methods of sample preparation. For example, Fig. 18.58 illustrates the method of air pluviation in which air-dry sand falls through a funnel with the height of fall maintained constant. The prepared sample is made denser by increasing the height of fall (gravity energy) or reducing the rate of fall (less grain-to-grain collision and energy loss) as Kolbuszewski (1948a, b) reported.

The density is controlled also by vibration or impacts (Fig. 18.59). This densification is performed by placing sand by layers (for example, 10 layers) and each layer is densified as illustrated in Fig. 18.59 to the desired relative density (Sect. 1.2). Usually, the number of hammer impacts or tamping is held constant for all the layers. It is sometimes the case that less efforts are made for bottom layers because the bottom layers are somehow densified further when upper ones are compacted. The particular number of impacts for each layer is determined by trials-and-errors. Among these methods, the author prefers air pluviation with controlled height of sand fall because this method gives the most stable results (repeatability in test results).

Since shear tests assume uniform stress and strain states within a specimen, efforts are needed to achieve uniform density and uniform packing of sand grains as well. When sand is densified layer by layer as in Fig. 18.59, it is possible that lower layers are subject to more number and more extent of compaction than upper layers. To avoid this, Ladd (1978) proposed to carry out less extent of compaction for lower layers (undercompaction). Although some index was proposed by Ladd (1978) to achieve the best uniformity, its meaning is not clear. Anyhow, the variation in extent of compaction between lower and upper layers should be determined by trials-and-errors.

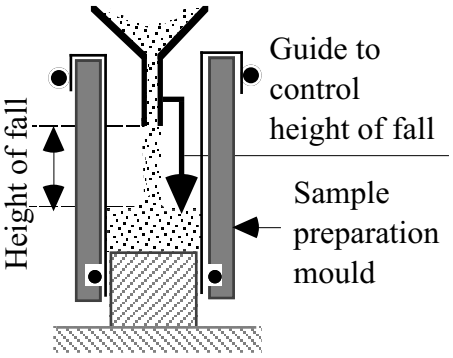

Fig. 18.58 Air pluviation technique of sample preparation

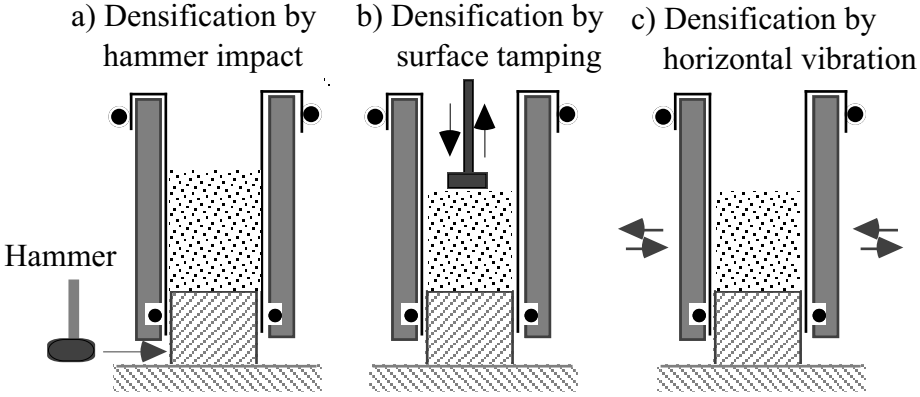

Fig. 18.59 Densification of sand sample

Another important issue in sample preparation is the extent of water saturation. In early days, a reasonably high extent of saturation was achieved by water-pluviation in which a sample preparation mould (Fig. 18.58) was filled with deaired water, and then sand, which was submerged in water, was slowly poured into the mould (Fig. 18.60a). Deaired water means distilled water (pure water without solution of gas) that is placed under vacuum for at least several hours so that dissolved gas may be removed. Deaired water is expected to have less risk to generate air bubble in the pore of a soil sample.

Another problem to affect water saturation is the migration of molecules of pressurized air (N_2 and O_2) through the pressurized water in the triaxial chamber and then through molecular holes of a rubber membrane. Since the water in the chamber is under higher pressure, no bubble occurs. Once the gas

molecules come into a soil specimen, the pore water is subject to lower pressure, and the dissolved gas is turned to bubbles. This is a problem during long-term consolidation (maybe longer than ten days). To avoid this, it is necessary to pressurize the chamber water by balloons, which prevents any contact of water and air. Use of mercury as the chamber liquid is useful. However, mercury may give health problems to experimentalists.

More recently, the degree of saturation has been improved either by (1) pluviation of CO_2 gas (during sample preparation) (Fig. 18.60b) and circulating CO_2 gas from bottom to top of a sample followed by deaired water or by (2) removal of pore air by vacuum (Fig. 18.60c). In the vacuum method, the pore pressure is made approximately equal to –98 kPa. To maintain the effective stress at a low level in this stage of sample preparation, the external pressure (total stress or chamber pressure) is reduced as well to, for example, –78 kPa, so that the effective stress is maintained at –78 kPa – (–98 kPa) = 20 kPa. Skempton´s B value (Sect. 18.16) is desired to be not less than 0.95 as a criterion of water-saturation. It is, however, easy to achieve $B>0.98$ after some experiences.

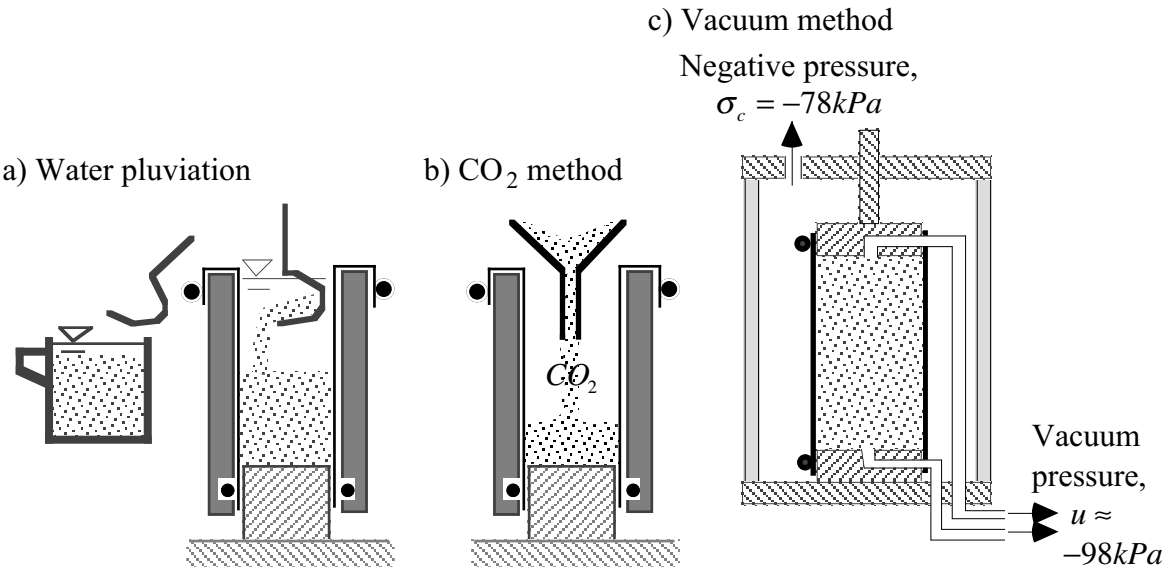

Fig. 18.60 Measures to help achieve high degree of water saturation

Different methods of sample preparation give different resistance to liquefaction. Mulilis et al. (1977) prepared sand samples by vibration of wet sand, tamping of wet sand, and pluviation of dry sand, and conducted liquefaction tests in order to find different liquefaction resistance. They further conducted microscopic studies on grain-to-grain contacts and discussed their statistic nature. It was also shown that sample preparation by layers results in layered structure in a sample. This is not a very good situation because uniformity within a sample body is always desired. In this regard, Miura and Toki (1982) proposed multiple sieve pluviation technique in which dry sand falls continuously through several sieves prior to deposition in a sample preparation mould.

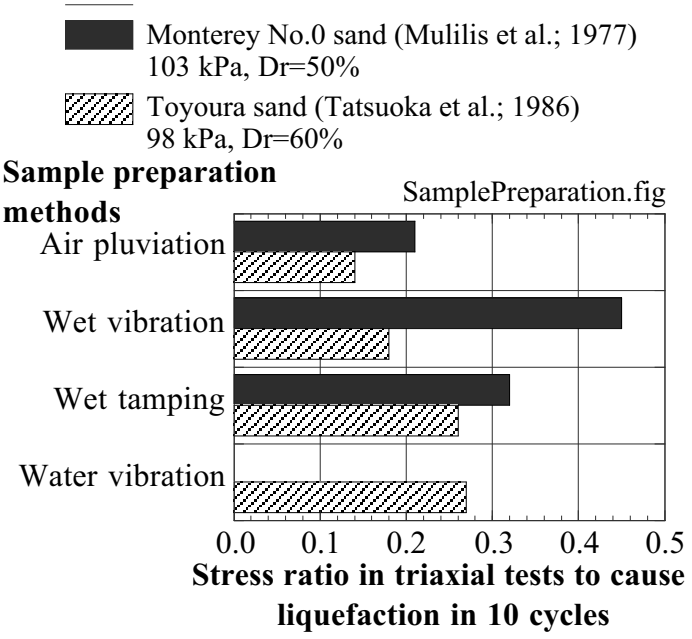

Fig. 18.61 Effects of sample preparation methods on liquefaction resistance of sand specimens

Tatsuoka et al. (1986) carried out experimental studies as well. Their results together with those by Mulilis et al. (1977) are shown in Fig. 18.61. It is seen therein that air pluviation produces the least liquefaction resistance (Chap. 19), while vibration or tamping leads to higher resistance. Air pluviation reproduces grain-to-grain contacts (microscopic granular structure) under gravity field. This condition is similar to what happens in real sedimentation process. More recently, Ghionna and Porcino (2006) obtained similar liquefaction resistance from frozen undisturbed samples (Sect. 10.20) and water-pluviation samples.

The effects of stress state during consolidation of a sand specimen was investigated by Yamashita et al. (1990). Thus, many studies have been made on the effects of sample preparation method on measured liquefaction resistance. Note, however, that no sample preparation method can precisely reproduce the natural geological procedure that consists not only of sedimentation process but also stress history and ageing effects (Sect. 18.13). This is the reason why collecting undisturbed soil samples is always important.

List of References in Chapter 18

Ambraseys, N.N. (1988) Engineering Seismology, Earthq. Eng. Struct. Dynam., Vol. 17, No. 1, pp. 1–105.

Atwater, B.F. (1992) Geologic evidence for earthquakes during the past 2000 Years along the Copalis River, Southern Coastal Washington, J. Geophys. Res., Vol. 97, B2, pp. 1901–1919.

Chillarige, A.V., Morgenstern, N.R., Robertson, P.K. and Christian, H.A. (1997) Seabed instability due to flow liquefaction in the Fraser River delta, Canadian Geotechnical Journal, Vol. 34, pp. 520-533.

Eginitis, D. (1895) Le tremblement de terre de Constantinople du 10 juillet 1894, Annales de Geographie, Vol. 4, pp. 151–165 (in French).

Elton, D.J. and Hamou, T.H. (1990) Liquefaction potential for Charleston, South Carolina, J. Geotech. Eng., ASCE, Vol. 116, No. 2, pp. 244–265.

Florin, V.A. and Ivanov, P.L. (1961) Liquefaction of saturated sandy soils, Proc. 5th Int. Conf. Soil Mech. Found. Eng., Vol. 1, pp. 107–111.

Galli, P. (2000) New empirical relationships between magnitude and distance for liquefaction, Tectonophysics, No. 324, pp. 169–187.

Ghionna, V.N. and Porcino, D. (2006) Liquefaction resistance of undisturbed and reconstituted samples of a natural coarse sand from undrained cyclic triaxial tests, J. Geotech. Geoenv. Eng., ASCE, Vol. 132, No. 2, pp. 194–201.

Hamada, M., Wakamatsu, K., Tazoh, T. and Yoshida, N. (1991) Soil liquefaction and resulting damage to structures during the July 16, 1990 Philippine earthquake, Tsuchi-to-Kiso, Month. Magazine, Jpn. Geotech. Soc., Vol. 39, No. 2, pp. 51–56 (in Japanese).

Jouanna, P., Mabssout, M. and Abellan, M.-A. (2000) Thermal signature of in situ soil damping under severe seismic actions, Soil Dynam. Earthq. Eng., Vol. 19, pp. 55–64.

JSSMFE (1966) Brief explanation on pictures taken at the moment of Niigata Earthquake, Soils Found., Vol. 6, No. 1, pp. i–vi.

Keefer, D.K. (1984) Landslides caused by earthquakes, Geol. Soc. Am. Bull., Vol. 95, pp. 406–421.

Kolbuszewski, J.J. (1948a) General investigation of the fundamental factors controlling loose packing of sands, Proc. 2nd Int. Conf. Soil Mech. Found. Eng., Vol. 1, pp. 47–49.

Kolbuszewski, J.J. (1948b) An experimental study of the maximum and minimum porosities of sands, Proc. 2nd Int. Conf. Soil Mech. Found. Eng., Vol. 1, pp. 158–165.

Kubo, K., Sugiyama, T. and Yasuda, S. (1979) Sites of liquefaction in Kawasaki City during 1923 Kanto earthquake 関東地震時の川崎市における液状化地点, Proc. 14th National Conf., Jpn Soc. Soil Mech. Found. Eng., pp. 1289–1292 (in Japanese).

Kuribayashi, E. and Tatsuoka, F. (1975) Brief review of liquefaction during earthquake in Japan, Soils Found., Vol. 15, No. 4, pp. 81–92.

Ladd, R.S. (1978) Preparing test specimens using undercompaction, Geotech. Test. J., Vol. 1, No. 1, pp. 16–23.

Maslov, N.N. (1957) Questions of seismic stability of submerged sandy foundations and structures, Proc. 4th Int. Conf. Soil Mech. Found. Eng., Vol. 1, pp. 368–372.

Miura, S. and Toki, S. (1982). A sample preparation method and its effect on static and cyclic deformation -strength properties of sand, Soils Found., Vol. 22, No. 1, pp. 61–77.

Mulilis, J.P., Mori, K., Seed, H.B. and Chan, C.K. (1977) Resistance to Liquefaction due to Sustained Pressure, Proc. ASCE, Vol. 103, GT7, pp. 793–797.

Mulilis, J.P., Seed, H.B., Chan, C.K., Mitchell, J.K. and Arulanandan, K. (1977) Effects of sample preparation on sand liquefaction, Proc. ASCE, Vol. 103, GT2, pp. 91–107.

Obermeier, S.F., Gohn, G.S., Weems, R.E., Gelinas, R.L. and Rubin, M. (1985) Geologic evidence for recurrent moderate to large earthquakes near Charleston, South Carolina. Science, Vol. 227, pp. 408–411.

Saito, Y. (1993) Sequence in continental shelf in Pacific Ocean off North East Japan, Chikyu Monthly, Special Issue 8 on Symposium on Events, Rhythm, and Their Records, pp. 80-85 (in Japanese).

Sangawa, A. (1992) Paleoliquefaction detected in archaeological sites, Tsuchi-to-Kiso Month. Magazine, Jpn. Geotech. Soc., Vol. 40, No. 1, pp. 13–18 (in Japanese).

Sangawa, A (1997) Shaking ground - seismic history of Japanese Archipelago, Doubou-Sha, ISBN4-8104-2363-8 C0021, p. 20 (in Japanese) (寒川旭：揺れる大地－日本列島の地震史－、同朋舎).

Seed, H.B. (1979) Soil liquefaction and cyclic mobility evaluation for level ground during earthquakes, Proc. ASCE, Vol. 105, GT2, pp. 201–255.

Seki, S., Mori, S. and Tachibana, H. (1992) Study on liquefaction and ageing effects in archaeological sites at Yuhigahama of Kamakura, Proc. 47th Ann. Conv. JSCE, Vol. 3 (in Japanese).

Shahnazari, H. and Towhata, I. (2002) Torsion shear tests on cyclic stress-dilatancy relationship of sand, Soils Found., Vol. 42, No. 1, pp. 105–119.

Sivathayalan, S. and Vaid, Y.P. (1998) Truly undrained response of granular soils with no membrane-penetration effects, Can. Geotech. J., Vol. 35, No. 5, pp. 730–739.

Skempton, A.W. (1954) The pore pressure coefficients A and B, Geotech., Vol. 4, No. 4, pp. 143–147.

Sundarraj, K. Prasad (1996) Evaluation of deformation characteristics of 1-G model ground during shaking using a laminar box, Doctoral thesis, University of Tokyo, p. 238.

Talwani, P. and Cox, J. (1985) Paleoseismic evidence for recurrence of earthquake near Charleston, South Carolina. Science, Vol. 229, pp. 379–381.

Talwani, P. and Schaeffer, W.T. (2001) Recurrence rates of large earthquakes in the South Carolina coastal plain based on paleoliquefaction data, J. Geophys. Res., Vol. 106, pp. 6621–6642.

Tatsuoka, F., Kimura, H., Pradhan, T.B.S. (1988) Liquefaction strength of sands subjected to sustained pressure, Soils Found., Vol. 28, No. 1, pp. 119–131.

Tatsuoka, F., Ochi, K., Fujii, S. and Okamoto, M. (1986) Cyclic undrained triaxial and torsional shear strength of sands for different sample preparation methods, Soils Found., Vol. 26, No. 3, pp. 23–41.

Towhata, I., Ishihara, K., Kiku, H., Shimizu, Y. and Irisawa, T. (2001) Submarine slides and land settlements in coastal areas during Kocaeli earthquake, Proc. Earthq. Geotech. Eng. Satellite Conf., XVth Int. Conf. Soil Mech. Geotech. Eng., Istanbul, Turkey, pp. 71–76.

Towhata, I., Prasad, S.K., Honda, T. and Chandradhara, G.P. (2001) Geotechnical reconnaissance study on damage caused by 2001 Gujarat earthquake of India, Soils Found., Vol. 42, No. 4, pp. 77–88.

Tsukuda, T. (1995) Precursor and Prediction of Big Earthquake, Asahi News Shop series, p. 46.

Tuttle, M., Law, K.T., Seeber, L. and Jacob, K. (1990) Liquefaction and ground failure induced by the 1988 Saguenay Quebec Earthquake, Can. Geotech. J., Vol. 27, pp. 580–589.

Wakamatsu, K. (1993) In Report on the July 16, 1990, Luzon earthquake, the Philippines, JSCE, pp. 170–173.

Wakamatsu, K. (1991) Map of historical liquefactions in Japan, University of Tokai Press (in Japanese).

Wakamatsu, K. (1993) In Report on the July 16, 1990, Luzon earthquake, the Philippines, JSCE, pp. 170–173.

Wichtmann, T., Niemunis, A., Triantafyllidis, Th. and Poblete, M. (2005) Correlation of cyclic preloading with the liquefaction resistance, Soil Dynam. Earthq. Eng., Vol. 25, pp. 923–932.

Yamashita, S., Toki, S. and Miura, M. (1990) Change of liquefaction behaviour in sand with anisotropic fabric due to anisotropic consolidation history, Soils Found., Vol. 30, No. 2, pp. 167–178 (in Japanese).

Yoshimi, Y. (1967) An experimental study of liquefaction of saturated sands, Soils Found., Vol. 7, No. 2, pp. 20–32.

Youd, T.L. (1977) Discussion of "Brief review of liquefaction during earthquakes in Japan," Soils Found., Vol. 17, No. 1, pp. 82–85.